Accepted Manuscript

New comprehensive studies of a gold(III) Dithiocarbamate complex with proven anticancer properties: Aqueous dissolution with cyclodextrins, pharmacokinetics and upstream inhibition of the ubiquitin-proteasome pathway

Marianna F. Tomasello, Chiara Nardon, Valeria Lanza, Giuseppe Di Natale, Nicolò Pettenuzzo, Stefano Salmaso, Danilo Milardi, Paolo Caliceti, Giuseppe Pappalardo, Dolores Fregona

PII: S0223-5234(17)30459-2

DOI: 10.1016/j.ejmech.2017.06.013

Reference: EJMECH 9508

To appear in: *European Journal of Medicinal Chemistry*

Received Date: 1 March 2017

Revised Date: 4 May 2017

Accepted Date: 6 June 2017

Please cite this article as: M.F. Tomasello, C. Nardon, V. Lanza, G. Di Natale, Nicolò. Pettenuzzo, S. Salmaso, D. Milardi, P. Caliceti, G. Pappalardo, D. Fregona, New comprehensive studies of a gold(III) Dithiocarbamate complex with proven anticancer properties: Aqueous dissolution with cyclodextrins, pharmacokinetics and upstream inhibition of the ubiquitin-proteasome pathway, *European Journal of Medicinal Chemistry* (2017), doi: 10.1016/j.ejmech.2017.06.013.

AuL12

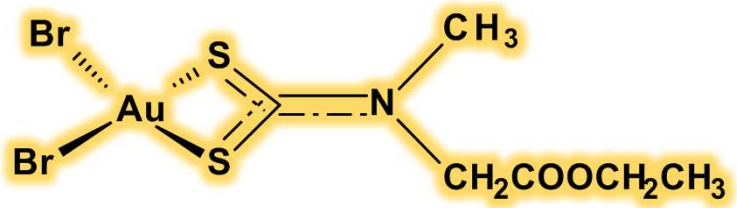

In cell proteasome inhibition

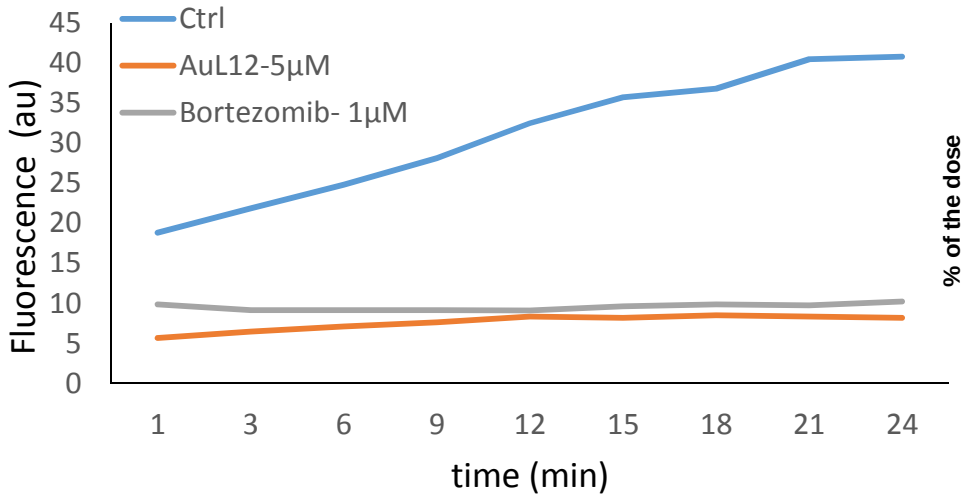

In vivo delivery and stability

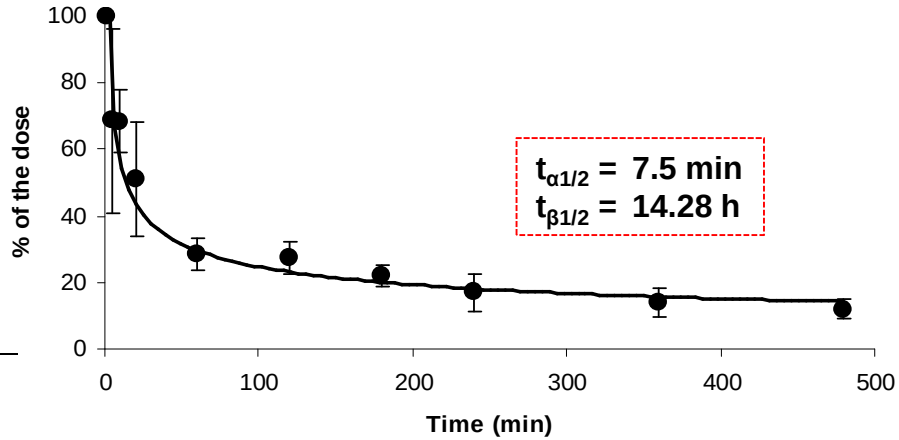

New comprehensive studies of a gold(III) Dithiocarbamate complex with proven anticancer properties: aqueous dissolution with cyclodextrins, pharmacokinetics and upstream inhibition of the ubiquitin-proteasome pathway

Marianna F. Tomasello,[†,#] Chiara Nardon,[‡,#] Valeria Lanza,[†] Giuseppe Di Natale,[†] Nicolò Pettenuzzo,[‡] Stefano Salmaso,[§] Danilo Milardi,[†] Paolo Caliceti,[§] Giuseppe Pappalardo,* and Dolores Fregona[‡,*]

[†] IBB-CNR, Istituto di Biostrutture e Bioimmagini, Sede Secondaria di Catania, Via Paolo Gaifami, 18 - 95126 Catania, Italy

[‡] Università degli Studi di Padova, Dipartimento di Scienze Chimiche, Via F. Marzolo 1, 35131, Padova, Italy

[§] Università degli Studi di Padova, Dipartimento di Scienze Farmaceutiche, Via F. Marzolo 5, 35131, Padova, Italy

# these authors contributed equally to this work.

* corresponding authors: Dolores Fregona, E-mail: dolores.fregona@unipd.it; Giuseppe Pappalardo, E-mail: giuseppe.pappalardo@cnr.it

ABSTRACT

The gold(III)-dithiocarbamate complex AuL12 (dibromo [ethyl-*N*-(dithiocarboxy-kS,kS')-*N*-methylglycinate] gold(III)), is endowed with promising in vitro/in vivo antitumor activity and toxicological profile. Here, we report our recent strategies to improve its water solubility and stability under physiological conditions along with our efforts for unravelling its tangled mechanism of action. We used three types of α-cyclodextrins (CDs), namely β-CD, Me-β-CD and HP-β-CD to prepare aqueous solutions of AuL12. The ability of these natural oligosaccharide carriers to enhance water solubility of hydrophobic compounds, allowed drug stability of AuL12 to be investigated. Moreover, pharmacokinetic experiments were first carried out for a gold(III) coordination compound, after i.v. injection of the nanoformulation AuL12/HP-β-CD to female mice. The gold content in the blood samples was detected at scheduled times by AAS (atomic absorption spectrometry) analysis, highlighting a fast biodistribution with a $t_{\beta 1/2}$ of few minutes and a slow escretion ($t_{\alpha 1/2}$ of 14.3 h). The in vitro cytotoxic activity of AuL12 was compared with the AuL12/HP-β- CD mixture against a panel of three human tumor cell lines (*i.e.*, HeLa, KB and MCF7). Concerning the mechanism of action, we previously reported the proteasome-inhibitory activity of some our gold(III)-based compounds. In this work, we moved from the proteasome target to upstream of the important ubiquitin-proteasome pathway, testing

the effects of AuL12 on the polyubiquitination reactions involving the Ub–activating (E1) and –conjugating (E2) enzymes.

KEYWORDS: gold complexes, anticancer agents, cyclodextrin, proteasome inhibitors

1. Introduction

Based on the known antitumor properties and poor toxicological profile of the drug cisplatin (Figure 1A) and its analogues,[1-3] our previous work on new metal-based anticancer agents has highlighted promising chemotherapeutic indexes for a number of gold(III)-dithiocarbamato complexes. Data collected so far for this class of potential antiblastic drugs have been exhaustively reviewed in some recent review papers.[4,5] AuL12 (dibromo[ethyl-*N*-(dithiocarboxy-*k*S,*k*S')-*N*-methylglycinate] gold(III), Figure 1B) is one of our most interesting compounds in terms of *in vitro*/*in vivo* anticancer activity and systemic toxicity. Nevertheless, its poor biopharmaceutical properties, namely water-solubility and stability,[6] may prevent its future pharmaceutical development. Therefore, we have recently started to investigate new biocompatible nanocarriers able to enhance the AuL12 solubility in aqueous media along with maintaining or improving the anti-proliferative profile. AuL12 was formulated within 1,2-distearoyl-sn-glycero-3- phosphoethanolamine-*N*-[amino(polyethylene glycol)-2000] (DSPE-PEG2000) and Pluronic® F127 (PF127) micelles. Both micelle systems were found to be suitable vehicles for AuL12. [7,8] Furthermore, the addition of a bombesin peptide analogue or the octapeptide CCK8 to the micelle surface endowed the AuL12 nanomedicines with cancer-targeting properties, which resulted in enhanced *in vitro* selective antiproliferative activity. [7,8] Based on these promising results, cyclodextrin-based formulations were lately investigated.

Cyclodextrins (CDs) are natural and semisynthetic cyclic oligomers formed by 6-8 D-(+)-glucopyranosyl units linked by α-1,4-glycosidic bonds. These cone frustum-shaped molecules consist of an external hydrophilic surface exposing primary and secondary hydroxyl groups along the ring edge and an internal lipophilic cavity with glycosidic oxygen and methine. [9,10] As a result, CDs can form inclusion complexes with various hydrophobic compounds, increasing their chemical stability,

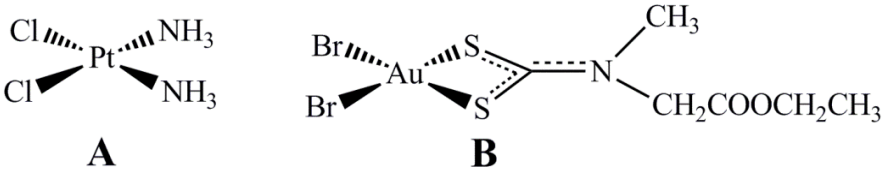

Figure 1. Chemical structures of the antitumor drug cisplatin (A) and of the complex AuL12 (B).

solubility and bioavailability. [9-11] In this work, we took into account β-cyclodextrins (β-CD) and their randomly-substituted derivatives methyl-β-cyclodextrins (Me-β-CD) and (2-hydroxypropyl)-β-cyclodextrins (HP-β-CD), studying the corresponding AuL12-solubilizing and -stabilizing capabilities along with the in vitro antitumor activity against the three human tumor cell lines HeLa, KB and MCF7 (24-h treatment). Moreover, pharmacokinetics (PK) of AuL12 was investigated for the first time. Studies on pharmacokinetic properties of metal-based compounds are rare and, to date, they are focused only on platinum-, ruthenium-, copper-, titanium-, bismuth-, technetium- and tin-containing derivatives. [12-19] It is worth highlighting that, as far as we know, this is the first paper reporting PK for gold(III) coordination compounds, as the clinically-established drugs auranofin (1-Thio-β-D-glucopyranosatotriethylphosphine gold(I)-2,3,4,6-tetraacetate), aurothioglucose and the sodium aurothiomalate contain gold(I) centers.[17, 20-21]

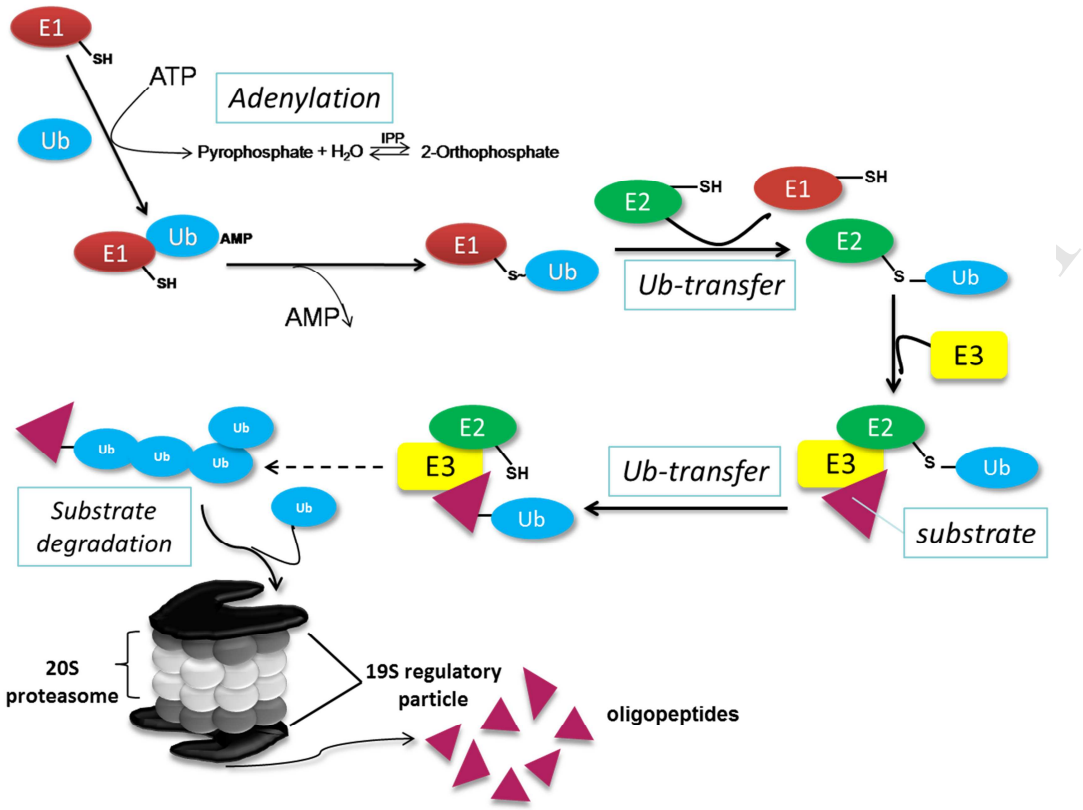

Figure 2. The ubiquitin-proteasome system: E1 is the ubiquitin-activating enzyme recruiting ubiquitin, E2 is the ubiquitin-conjugating enzyme that transfers the ubiquitin to the targeted protein while E3 is the ubiquitin-ligase acting as a scaffold protein that interacts with the E2 enzyme for transferring ubiquitin to the target protein (E3 ubiquitin-ligases can either promote the direct transfer of ubiquitin from E2 to the substrate or interact with the cognate E2, followed by the formation of a thioester bond with ubiquitin and subsequent transfer of ubiquitin to the substrate). The whole process is reversible through the action of deubiquitinases (DUBs) that remove ubiquitin chains linked to the target protein. During substrate protein degradation, DUBs also process and recycle ubiquitin.

A further goal of this work is to unveil the mechanism of action of the complex AuL12. In the last years, proteasome inhibitors have emerged as promising anticancer antiproteasome drugs.[22-25] In fact, after the FDA-approval of bortezomib ([(1R)-3-methyl-1-[[(2S)-3-phenyl-2-(pyrazine-2-carbonylamino)propanoyl]amino]butyl]boronic acid) for the treatment of multiple myeloma in 2003, mounting evidence suggests that proteasome inhibitors are good

chemotherapeutics able to induce cell death in malignancies, thus prompting further development of new proteasome inhibitors.[26-28] In this regard, inorganic compounds stand out among others due to the inherent presence of an electrophilic trap (*e.g.*, a metal or semimetal center), required for inhibiting the catalytic pockets of proteasome.[24] The 26S (or more properly 30S) proteasome is a large multi-subunit protease able to identify and hydrolyze, both in the nucleus and in the cytosol, the proteins labeled with a chain of ubiquitin molecules. The central part of the 26S complex, the 20S proteasome, is the actual proteolytic machine as it contains multiple peptidase activities (*i.e.*, chymotrypsin(CT)-, trypsin(T)- and caspase(PGPH)-like).[29] Two regulatory particles (19S units) recognize and deubiquinate the target proteins, and translocate them into the catalytic 20S core for degradation into oligopeptides (Figure 2). The ubiquitin-proteasome system (UPS) relies on the sequential actions of three enzymes - the ubiquitin-activating enzyme (E1), the ubiquitin-conjugating enzyme (E2) and the ubiquitin-protein ligase (E3) - which result in the formation of the polyubiquitin chain.[29-32] Therefore, low-molecular weight agents able to selectively inhibit the proteasome 20S core and/or to act at multiple levels of the ubiquitination cascade offer a great deal of potential in destabilizing the UPS.[33] As an example, the development of novel E1 or E2 inhibitors has been growing in therapeutic interest. In particular, E1 inhibition has been supposed to prevent ubiquitination and thus to overall block the UPS with similar effects to proteasome inhibition.[34,35] For instance, a number of studies, aimed at targeting the active site of E1 enzymes, produced new compounds that stabilize the "genome guardian" p53, changing the levels of pro- and anti-apoptotic ubiquitinated proteins and, hence, leading to tumor growth inhibition in murine cancer models.[34,35]

Based on the proteasome-inhibitory properties found for a number of our Au(III) dithiocarbamate complexes,[36-38] the monitoring of the enzymatic activity at the (intra)cellular

level is a step forward. A variety of fluorescent probes have been developed to assess proteasome function in living cells. [39-41] In this work, we show the multi-level effects of AuL12 on UPS by using two different approaches. The first one was aimed at determining the compound influence on the E1/E2-catalysed poly-ubiquitination reaction whereas the second strategy was focused on the use of the internally-quenched fluorogenic peptide TED (TAT-EDANS-DABCYL), [42] specifically recognized and hydrolyzed by the proteasome, to elucidate the drug effects directly on the multicatalytic enzyme at the single-cell level.

2. Materials and methods

2.1 General informations

β-cyclodextrins (β-CD) and methyl-β-cyclodextrin (Me-β-CD) have been kindly gifted by Roquette (Lestrem, France). (2-hydroxypropyl)-β-cyclodextrin (HP-β-CD) - average degree of substitution (DS) 4.3 - nitric acid and hydrochloride acid TraceSELECT® were purchased from Fluka Chemika (Buchs, Switzerland). Dimethylsulfoxide (DMSO) and Tween 20 were obtained from Sigma Aldrich. Ubiquitin from bovine erythrocytes was purchased from Biomol International and purified by dialysis against pure water overnight at 20 °C. Protein concentration in pure water was routinely checked by UV (ε_{280} = 1280 M^{-1} cm^{-1}). [43,44] Human recombinant Ub-activating Enzyme (E1) and Ub-conjugating Enzyme (E2-25K) were purchased from Boston Biochem. Standard solutions of di-ubiquitin (Ub_2), tri-ubiquitin (Ub_3), tetra-ubiquitin chains (Ub_4), Lys48-linked Ub were purchased from ENZO Life Sciences. For SDS PAGE, NuPAGE® Novex® Bis-Tris gels and 2-(*N*-morpholino) ethanesulfonic acid (MES) buffer were obtained from Invitrogen. For Western blotting, mouse anti mono- and poly-ubiquitinylated conjugates,

mAb (FK2) and goat anti-mouse IgG1-HRP antibody were obtained from ENZO Life Science and Santa Cruz Biotechnology, respectively. For crosslinking experiments, bis (sulfosuccinimidyl)suberate (BS3) was purchased from Sigma-Aldrich. The MALDI matrix 3,5-Dimethoxy-4-hydroxycinnamic acid (sinapinic acid, SIN) was purchased from Sciex and used without further purification. BSA, IgG and Peptide Mass Standard Calibration Kits were purchased from Sciex. The Ubiquitylation assay kit containing 20x ubiquitin-activating enzyme solution (E1) (2 µM), 20x ubiquitin solution (Ub) (50 µM), 20x Mg-ATP solution (0.1 M) and 10x ubiquitinylation buffer (Tris(Hydroxymethyl)aminomethane, TRIS buffer) were purchased from Abcam. Inorganic pyrophophatase (IPP) and Dithiothreitol (DTT) were purchased from Sigma-Aldrich. Acetonitrile (ACN) and Trifluoroacetic acid (TFA) (mass spectrometry grade) were purchased from Fisher Scientific. All aqueous solutions were prepared using a Barnstead NanoPure system with a 0.2 µm membrane filter (Thermo Scientific). Reagents for cell culture were obtained from Life Technologies (formerly invitrogen). 3-(4,5-dimethylthiazole-2-yl)-2,5-diphenyltetrazolium bromide (MTT) and the tissue culture products were obtained from Sigma Chemical Co. (St. Louis, MO, USA).

2.2 Chemical and biophysical properties

2.2.1 AuL12 synthesis and characterization

AuL12 was synthesized in water at room temperature starting from commercial sarcosine ethyl ester, according to our previously reported procedure [45], purified (purity >96%), analyzed by elemental analysis and chromatography and fully characterized to confirm its stoichiometry.

2.2.2 AuL12 solubility and stability

An AuL12 solution in DMSO (0.5 mg/mL) was serially diluted with DMSO and analysed by UV-Vis to calculate the molar extinction coefficient ($\varepsilon_{1/100}$) and by RP-C18 chromatography using a 4.6x250 mm Phenomenex Luna C18 column (Torrance, CA, USA) eluted with a gradient of water/0.05% trifluoroacetic (eluent A) and acetonitrile/0.05% trifluoroacetic (eluent B) as follows: 0-18 min: 30% eluent B; 18-24 min from 30% to 95% eluent B. The UV detector was set at 265 nm. The drug content in the solutions was determined according to the peak area, which was referred to the titration curve obtained by the analysis of DMSO solutions containing known AuL12 concentrations {peak area = 9890.2 [(AuL12) µM] + 99546; R^2=0.98}.

For solubility and stability studies, 5 mg of AuL12 were dissolved in 0.5 mL DMSO and then centrifuged and analyzed by UV-Vis spectrophotometry and by RP-HPLC. 50 µl of the organic solution were added to 950 µL of: 1. 0.06 M acetate buffer, 0.15 M NaCl, pH 4.5, 2. 0.01 M phosphate buffer, 0.15 M NaCl, pH 7.4; 3. 0.03 M HEPES, 0.15 M NaCl, pH 8.5. At scheduled times, the DMSO and buffer solutions were centrifuged for 3 min at 10000 rpm and then analyzed by UV- Vis and RP-HPLC to calculate the AuL12 concentration. The precipitates were analyzed by atom absorption and ESI-TOF mass spectrometry.

2..2.3 AuL12 dissolution in cyclodextrins

Method A (co-solubilization). Samples were prepared by adding 30 µL solutions of 10 mg/mL AuL12 in DMF to 200 µL DMF solutions containing increasing concentrations of

β-CD (0-14 mg/mL), Me-β-CD (0-40 mg/mL) or HP-β-CD (0-40 mg/mL). The organic solvent was removed under vacuum and the solid residues were re-suspended in 200 µL of 0.06M sodium acetate buffer, 0.15 M NaCl, pH 4.5, and stirred for 10 min at room temperature. The samples were centrifuged at 10,000 rpm for 5 min and the supernatant was filtered with 0.22 µm cut-off filter. AuL12 in the solutions was assessed by RP-C18 chromatography as reported above.

Method B (direct dissolution). Samples were prepared by desiccating 30 µL of 10 mg/mL AuL12 in DMF under vacuum. The solid residues were re-suspended in 200 µL of 50 mM sodium acetate buffer, pH 4.5, containing increasing concentrations of β-CD (0-14 mg/mL), Me-β-CD (0-40 mg/mL) or HP-β-CD (0-40 mg/mL). The suspensions were gently mixed for 72 h at room temperature in the dark. The samples were centrifuged, filtered and the AuL12 concentration in the solutions was determined by RP-HPLC as reported above.

The solubility data obtained with the Method A for the three types of AuL12/CD inclusion complexes were processed to calculate the corresponding AuL12/CD apparent stability constants (K_c). Each K_c was obtained by the slope of the phase-solubility diagram according to the following equation: K_c= (slope)/[S_0(1-slope)] where S_0 is the saturation concentration of AuL12 in buffer without cyclodextrins (60 µg/mL).

2.2.4 Drug degradation studies

AuL12/CD solutions (1 mL) were prepared according to the Method A by mixing 150 µL of 10 mg/mL AuL12 in DMF with 1 mL of 40 mg/mL CD in DMF. The final solutions obtained by the dissolution process were lyophilized and then the dry product

was added of phosphate buffer at pH 7.4. The suspension was stirred for 10 min. After centrifugation at 6000 rpm for 4 min, the supernatant was incubated at 37°C. At scheduled times, 50 µL aliquots were then withdrawn and analysed by RP-HPLC according to the procedure reported above.

2.3 Biological evaluation

2.3.1 Cell culture studies

For the *in vitro* experiments related to the evaluation of antitumor activity of AuL12-encapsulating supramolecular aggregates, human nasopharyngeal epidermal carcinoma KB cells, human breast adenocarcinoma MCF7 cells and human cervical carcinoma HeLa cells were cultured as a monolayer at 37 °C in a humidified atmosphere containing 5% CO_2 in Dulbecco's modified Eagle's medium (DMEM) supplemented with 10% (v/v) heat-inactivated fetal bovine serum, 2 mM glutamine, 100 U/mL penicillin, 100 µg/mL streptomycin and 0.25 µg/mL of Amphotericin B. Cells were routinely treated with a 500 µg/mL trypsin and 200 µg/mL EDTA solution in Ca^{2+} and Mg^{2+} free phosphate buffered saline (PBS).

For the *in vitro* experiments related to the evaluation of proteasome-inhibitory activity of AuL12, MCF7 cells were cultured in RPMI-1640 supplemented with 10% heat-inactivated FBS, 100 U/mL penicillin, and 100 µg/mL streptomycin and maintained under 5% CO_2 in humidified air at 37°C. Once reached 95% confluence, cells were split (by using 0.25% trypsin-EDTA) into fractions and propagated or used in experiments. 24 hours after seeding, cells were exposed to various concentrations of AuL12 for 6 hours. Exposure to 1 µM bortezomib for 6 hours was used as a positive control.

2.3.2 Cytotoxicity assays

For the *in vitro* experiments related to the evaluation of antitumor activity of AuL12 in different vehicles, KB, MCF7 and HeLa cells were seeded in 96-well tissue culture plates at a density of 6×10^3 cells/well. After 24 h, the culture medium was replaced with 100 µL of medium containing increasing concentrations (in the µM domain) of AuL12 (pre-dissolved in DMSO) or equivalent drug concentrations of a 1:5 AuL12/HP-β-cyclodextrin molar ratio solution prepared according to Method A. The final DMSO content in the assayed samples was always lower than 0.5% v/v. After the appropriate incubation time (24 h or 6 h for the experiments associated with the AuL12 proteasome-inhibitory activity), for each well the medium was replaced with fresh medium containing 0.5 mg/mL MTT and incubated at 37°C for 2 hours (MTT assay exploits the reduction of the tetrazolium salt MTT to purple formazan crystals in living cells). [46] The produced formazan crystals were dissolved by using DMSO, and the absorbance (λ = 569 nm) was measured using the top reading mode of a Varioskan flash spectral scanning multimode microplate reader (Thermo Scientific), and/or a Bio-Tek Instruments microplate autoreader EL311SK (Highland, Vermont, USA), with a reference λ of 670 nm to subtract background.

2.3.3 Evaluation of AuL12 uptake

In order to evaluate the mechanism by which AuL12 is up-taken by cells, we adopted two different experimental approaches. In the first approach, MCF7 cells were incubated in the presence of increasing concentrations (0.5-20 µM) of AuL12 or Bortezomib (1 µM) at 4 °C for 60 minutes. Cell incubation was then extended for additional five hours, after

the removal of the compounds. Pre-incubation with cytochalasin, an inhibitor of endocytosis, was the second used method: MCF7 cells were pre-incubated for 1h in the presence of cytochalasin and, after that, cells were exposed for 6 hours to increasing concentrations of AuL12 (0.5-20 µM) and Bortezomib (1 µM), as a control. We monitored, for both the experimental approaches above described, the effects related to AuL12 or bortezomib cellular uptake by measuring both cell viability and proteasome activity.

2.3.4 Pharmacokinetic studies

Four-week old female Balb/C mice, weighing 22-24 g, were obtained from the Dept. of Pharmaceutical and Pharmacological Sciences of the University of Padua. Animal care and handling were performed in accordance with the provisions of the European Economic Community Council Directive 86/209 (recognized and adopted by the Italian Government with the approval decree D.M. No. 230/95-B) and the NIH publication No. 85-23, revised in 1985. The animal experiments were approved by the ethical committee of the University of Padua and the Italian Institutions of control.

HP-β-CD (80 mg) were dissolved in 200 µL of DMF and the solution was added of AuL12 (4.4 mg). After complete dissolution, the organic solvent was removed under vacuum and the solid residue was dissolved in 2 mL of 0.01 M phosphate buffer, 0.15 M NaCl, pH 7.4, and stirred for 10 min at room temperature (Method A). The sample was centrifuged at 10,000 rpm for 5 min and the supernatant was filtered with 0.22 µm cut-off filter. Volumes of 100 µL were injected in the tail vein to 8 female BALB/c mice. At scheduled times, 50 µL of blood was withdrawn from the retro-orbital sinus. The blood

samples were digested with HNO_3/HCl 1:3 v/v ratio under heating at 90°C for 2 h. The samples were transferred into a 5 mL volumetric flask and brought to volume with 1% HCl. Quantitative analysis of gold was performed by Atomic Absorption Spectrometers (AAS) using Varian's AA240 with GTA120 graphite furnace and Zeeman background corrector, equipped with autosampler (Varian AA240 Zeeman, Varian Inc.). The experimental values were elaborated by Kinetica Software (Thermo Scientific™) according to bi-compartmental models.

2.3.5 Lys48 self-polyubiquitination reactions in test tubes

Lys48-linked polyubiquitination reactions were carried out at pH 7.4 (T=25°C) in small volumes (40 µL) of ligation buffer (50 mM TRIS, 5 mM $MgCl_2$, 30 µM DTT and 2 mM ATP) containing Ub (10 µM), E1 (500 nM) and E2-25K (1 µM). [47] All reactions were carried out in presence of different concentrations of AuL12, ranging from 0.5 to 7 µM. The reactions were quenched after 3-hour incubation with addition of 10 µL of the sample loading buffer containing 8% (w/v) SDS, 24% (v/v) glycerol, 0.015% Coomassie Blue G, and were size-fractioned by SDS-polyacrylamide gel electrophoresis. Samples were then electro-transferred onto a nitrocellulose membrane (GE Healthcare, Lifescience). The membranes were blocked with Odyssey blocking buffer for 1 hour and then incubated overnight at 4°C with K48-linkage specific polyubiquitin antibody. The membrane was washed thrice for 5 minutes with PBS-T (PBS-0.05% Tween-20) and then incubated with IRDye 800–labeled secondary antibody (1:12,000) from Molecular Probes (Eugene, OR) for 30 minutes. Membrane visualization was done using the LI-COR Odyssey IR Imaging System (LI-COR Biosciences, Lincoln). All blots were compared with a standard mix containing AuL12 (5 µM), di-ubiquitin (Ub_2), tri-ubiquitin (Ub_3), tetra-ubiquitin chains

(Ub_4), to ensure the full efficiency of antibodies in presence of AuL12. In order to rule out any possible undesired effect of DTT on the integrity of AuL12, we collected UV spectra of DTT/AuL12 mixtures at different molar ratios (Fig. S1). These experiments confirmed that DTT does not change the oxidation state of the Au complex under the experimental conditions adopted for poly-Ub chain synthesis.

2.3.6 Ubiquitin activation

The efficiency of Ub activation by E1 in the presence of AuL12 was monitored by measuring Ub adenylate formation using reaction mixtures containing 2.5 µM E1, 50 µM Ub, 2 mM ATP in 10 mM MgCl2, 50 mM TRIS, pH 7.5 as reported elsewhere. [48] Reaction mixtures were incubated with 3 and 5 µM AuL12 at 37°C for 30 min before an aliquot of the sample loading buffer (described above) was added to quench the reaction. The samples were then analyzed by SDS-PAGE under reducing conditions, transferred onto a nitrocellulose membrane (GE Healthcare, Lifescience), probed with mouse anti mono- and poly-ubiquitinylated conjugates mAb [clone FK2] (1:5,000), overnight at 4°C. After three washes for 5 minutes with PBS-T (PBS, 0.05% Tween 20), the membrane was incubated with IRDye 800–labeled anti-mouse secondary antibody (1:12,000) from Molecular Probes (Eugene, OR) for 30 minutes. Visualization of bands was performed on a Li-Cor Odyssey Imaging System (Li-Cor Biosciences, Lincoln, NE).

2.3.7 Crosslinking experiments

Ub (20 µM) was incubated on ice in 20 µL of 50 mM TRIS buffer (pH 7.4), $MgCl_2$ (5 mM) and the E2-conjugating enzyme (E2-25K) in the absence or in the presence of different concentrations of AuL12 (0.1-5 µM). After 3 hours, the chemical cross-linker

BS3 (0.3 mM) was added to the mixture, followed by overnight incubation at 0°C. Incubation was continued at 0°C overnight. Solutions were then kept for 1 hour at 20°C. Next, chemical crosslinking was quenched by dilution with the sample loading buffer (described above) and the aliquots were analyzed by SDS-PAGE. The gels were stained by the conventional silver staining procedure. [49]

2.3.8 Sample preparation and MALDI-TOF-MS

Sinapinic acid (SIN) matrix was prepared by dissolving 4-8 mg in 1 mL of aqueous solution containing 30% acetonitrile and 0.3% TFA. BSA and mouse IgG1 standard kits were used to calibrate the MALDI mass spectrometer for masses ranging from 60,000 to 200,000 Da, while bovine insulin, *E. coli* thioredoxin and horse apomyoglobin were used to cover a mass range from 4,000 to 20,000 Da. Lyophilized samples of IgG and BSA were dissolved in water and mixed with SIN at a final concentration of 0.6 pmol/µL. Lyophilized samples of bovine insulin, *E. coli* thioredoxin and horse apomyoglobin, used as mass standards, were dissolved in 3:7:0.01 acetonitrile/water/TFA at a final concentration of 0.5 pmol/µL, 2.75 pmol/µL and 4.0 pmol/µL, respectively. Activated (thioester linked) ubiquitin-E1 conjugate was generated by reaction of Ub and E1, in an Mg-ATP dependent process, in the presence of inorganic pyrophosphatase (IPP) and DTT (activating reaction solution). Briefly, IPP hydrolyzes the pyrophosphate produced by ubiquitin adenylation in the first step of the reaction while DTT ensures the reduced form of the E1 catalytic Cys attacking the ubiquitin-adenylate form (Fig. 3). Reagents were added according to the following order: 2.8 µL of ubiquitinylation buffer, 4 µL of IPP 100 U/mL in 20 mM Tris-HCl (pH 7.5), 1.2 µL of DTT 50 mM in 20 mM Tris-Cl (pH 7.5), 1 µL of Mg-ATP 0.1 M, 10 µL of E1 2 µM, 1 µLof Ub 50 µM.

Non-covalent adduct formation was investigated by mixing E1 and Ub (E1/Ub) in ubiquitinylation buffer (TRIS buffer). The final concentration of Ub and E1 in each sample was 2.5 µM and 1 µM, respectively. Each solution (20 µL) was incubated at 37 °C for 30 min. AuL12 stock solution ([AuL12]=1.82 mM) was prepared dissolving 1 mg in 1 mL methanol-water 50:50 %v/v. An AuL12 diluted solution ([AuL12]=0.182 mM) was obtained adding 100 µL of stock solution in 900 µL of water. When the inhibitory role of AuL12 was investigated, 0.548 µL of AuL12 diluted solution was added to the E1/Ub sample (E1/Ub/AuL12 in TRIS buffer).

Samples were analyzed using the "dried-droplet" MALDI sample preparation method, [50] that can be briefly described as follows: 1 to 2 µL of sample and 1 to 2 µL of matrix solution were mixed into a 0.5 mL tube, and 1 µL of this mixture was deposited on a stainless steel 384-well plate and dried at room-temperature.

MALDI-MS spectra were obtained using a 5800 MALDI-TOF/TOF mass spectrometer (Sciex) equipped with an automated single-plate sample-loading system, 1 kHz OptiBeam™ On-Axis Laser Nd:YAG 349 nm wavelength, delayed-extraction (DE), two acceleration regions, QuanTis™ Precursor Ion Selector, CID cell, two-stage reflector mirror and a 1000 MHz digitizer. The instrument was operated in linear high molecular weight mode (m/z range: 25,000-250,000) by applying the following voltages: 12 kV source 1, 11.5 kV Grid 1, 2.25 kV Source 1 Focus, 4.75 kV source 1 lens, 0.125 kV Y1 deflector, 0.072 kV Y2 Deflector, 0.032 kV X2 deflector, 5.25kV lens1, 3 kV linear detector. The same voltages were applied when operating in linear mid molecular weight mode (m/z range: 5,000-25,000) except for source 1 lens where a 4.25 kV voltage was used. Delayed extraction was used and the delay time was set according to the molecular

weight of the analyte to optimize resolution of its molecular ion. Mass spectra were acquired by averaging 300 to 800 shots. Laser pulse energy was adjusted according to the various MALDI matrices used.

2.3.9 Determination of proteasome inhibition by using the TED probe

At the end of each treatment, described above, cells were washed with PBS and pre-incubated with Phenol-red-free medium containing 50 µM TED (internally quenched fluorogenic peptide, TAT-EDANS-DABCYL) for 5 minutes to allow the probe to be internalized by cells. Cells were then transferred either on a confocal microscopy stage or on a microplate reader where the fluorescence emission of TED (exc. 340 nm/em. 510 nm) was followed over time. Fluorescence emission was recorded every 5 minutes up to 45 minutes, by using the "bottom reading" mode of a Varioskan flash spectral scanning multimode microplate reader (Thermo Scientific). When confocal time lapse was carried out, the fluorescence was measured as detailed below.

2.3.10 Imaging by confocal microscopy

Imaging of cells, plated in 35-mm glass-bottom cell culture dishes (Willco Wells), was carried out on an Olympus FV1000 confocal microscope, using a 63 Plan-Apo/1.4-NA oil-immersion objective. Standard one-confocal channel acquisitions (using one 1Photomultiplier detector kept at 510 nm) were made by using the 405 nm diode laser (50 mW). Single optical sections (0.42 µm z axis) through the middle of the cells were acquired for each field. Acquisitions were made each 3 minutes up to 30 minutes. The average fluorescence intensity for each cell was measured considering a series of ROI (region of interest) inside each single cell and by calculating the mean fluorescence

intensity (au) at the emission wavelength established by using the FV1000 software (release 2.0).

2.3.11 Statistical Analysis

Values are expressed as mean ± SEM. Statistical analysis was performed by one-way ANOVA with Tukey's post-hoc test. A P value <0.05 was taken as significant.

3. Results and Discussion

3.1 Chemical and biophysical properties

3.1.1 AuL12 solubility and stability.

Previous studies showed that the gold compound AuL12 is poorly soluble (logP=1.0) and undergoes rapid hydrolysis in aqueous media. [6,51] In this work, experiments carried out with different buffers (acetate, phosphate and HEPES) and pHs (4.5, 7.4 and 8.5) pointed out the solubility of AuL12 was about 0.1 mM regardless the dissolution buffer, while its stability was strongly affected by the value of the medium pH. Indeed, the UV-Vis spectrum of AuL12 in acetate buffer at pH 4.5 (Supporting Information Figure S1) was stable over 200 min, while it was found to change throughout the time at the other pHs, thus indicating the drug underwent hydrolysis in agreement with previous data. [6,51] In particular, the maximal absorbance peaks at 270 nm shifted to higher wavelengths and the maximal absorbance at 270 and 312 nm decreased. At pH 7.4 and 8.5, the spectra showed also a shoulder to peak 270 nm which was found to increase over time. The degradation rate of AuL12 in DMSO and at pH 4.5, 7.4 and 8.5 was determined by HPLC analysis. Supporting Information Figure

S2 shows that AuL12 was fairly stable at pH 4.5 without remarkable changes throughout 200 min. At this pH, the compound was even more stable than in DMSO where it was fairly soluble (>10 mg/mL). On the contrary, AuL12 rapidly degraded at physiological pH (pH 7.4) and at pH 8.5, producing a precipitate. The degradation of AuL12 in DMSO and buffers was found to occur according to a first-order kinetics. The rate constants (K_{obs}) in DMSO and in buffer at pH 4.5, 7.4 and 8.5 were $1x10^{-5}$, $3x10^{-6}$, $9x10^{-3}$ and $6x10^{-3}$ min^{-1}, respectively, indicating that the stability increases of about 103 times on passing from pH 7.4 to 4.5. The mass spectrum of AuL12 in acetate solution (Supporting Information Figure S3A) showed the presence of only one cationic species (exact mass: 581,00 Da) with a 1:2 metal-to-ligand ratio, formed under analysis conditions. In fact, this behavior is generally detected for all our gold(III) dithiocarbamate complexes when analyzed by ESI-MS. The same analysis carried out for the obtained precipitate in phosphate buffer (Supporting Information Figure S3 B) highlighted the presence of several molecular fragments derived from AuL12 degradation.

3.1.2 *AuL12 dissolution in cyclodextrins.*

In order to enhance the AuL12 solubility and stability at physiological pH, the coordination compound was formulated with cyclodextrins (CDs): β-cyclodextrins (β-CD), methyl-β-cyclodextrins (Me-β-CD) and hydroxypropyl-β-cyclodextrins (HP-β-CD). β-CD is the most common cyclodextrin. Nevertheless, β-CD is poorly soluble (18.5 g/L) and cannot be used for parenteral administration because of its toxicity.[52,53] Me-β-CD is more soluble and the presence of methyl groups extends the hydrophobic surface of the CD core, which can enhance the dissolution of hydrophobic molecules. [54] Finally, HP-β-CD has been approved for parenteral administration, which makes this CD the best candidate for the development of a pharmaceutical formulation of AuL12. [55,56] The molecular *in silico*

analysis performed with MarvinSketch software (ChemAxon, Cambridge, MA, USA) showed that about 80% of the van der Waals surface of AuL12 is hydrophobic and the molecular volume is 225 $Å^3$, which well fits the CD cavity volume (262 $Å^3$). [56]Thus, AuL12 solubility studies were carried out according to two different protocols: co-solubilization (Method A) and direct dissolution (Method B). The AuL12 association with CDs was found to change the UV-Vis profile of the drug. The maximal absorbance of the peak at 312 nm indeed decreased as the CD concentration in the solution increased. The phase-solubility profiles reported in Supporting Information Figure S4 describe the AuL12 solubility obtained at increasing CD concentrations. The solubility profiles were elaborated according to the method reported by Higuchi and Connors [57] to examine the ability of β-CD, Me-β-CD and HP-β-CD to form supramolecular complexes with AuL12. The profiles depicted in S4A (Method A) show that up to about 10 mM oligosaccharide concentrations, the three examined CDs yielded similar drug solubility with a 1:5 AuL12/CD molar ratio. The maximum cyclodextrin concentration depended on the oligosaccharide nature, the solubility of CD and the drug/CD complex. At the end-point of the low soluble β-CD, the AuL12 solubility was 1.72 mM, being 16-fold higher than its solubility in acetate buffer (about 0.1 mM). Due to their greater water solubility, Me-β-CD and HP-β-CD were investigated at higher concentrations than β-CD counterparts, though in both cases a drug solubility plateau was achieved at about 22 mM oligosaccharide concentration. Me-β-CD and HP-β-CD yielded 1.89 mM and 2.85 mM AuL12 solutions, respectively, which correspond to an increase of 17- and 26-fold compound solubility in comparison with the acetate buffer. If comparing the carriers, β-CD showed the lowest solubilizing capability with a 1.1- and 1.7-fold solubility increase on passing from them to Me-β-CD and HP-β-CD,

respectively. The solubility of AuL12 in the presence of HP-β-CD (the most soluble CD used in this study with a solubility of about 440 mM), linearly increased up to a carrier concentration of 22 mM when the maximal AuL12/HP-β-CD complex solubility was achieved. The phase-solubility profiles obtained by direct dissolution (Method B) and depicted in Figure S4B, show that this procedure is overall significantly less efficient in drug solubilization than the co-solubilization method (Method A, Figure S4A). Indeed, unexpectedly, Method B yielded an opposite solubilization trend compared to Method A. The maximal AuL12 solubility obtained with β-CD, Me-β-CD and HP-β-CD was 0.71, 0.54 and 0.29 mM, respectively, which corresponded to about 7-, 5- and 3-fold solubility increase with respect to the buffer without CDs. The maximal concentration of AuL12 was achieved at about 5, 12 and 15 mM CD concentration with β-CD, Me-β-CD and HP-β-CD, respectively. Intriguingly, the solubility profiles obtained by direct solubilization show that if further increasing CD concentration, a decrease in AuL12 solubility was obtained. This behavior was already observed with other guests, namely resveratrol, gliclazide and Ro 28-2653, a synthetic inhibitor of matrix metalloproteinases, and is due to the formation of insoluble supramolecular complexes with different stoichiometries. [58-61] According to these results, Method A was selected for the preparation of the AuL12/CDs complexes for the subsequent studies. Table 1 collects the apparent stability constants (K_c) of AuL12/CD supramolecular complexes obtained by elaboration of the solubility profiles associated with the co-solubilization (Method A). These data show that the AuL12/β-CD complex is the most stable while the AuL12/Me-β-CD and AuL12/HP-β-CD were about 4-8 times less stable than the latter.

	Inclusion apparent constant K_c (M^{-1})	**Degradation kinetic constant $k_{obs} \times 10^{-4}$(min^{-1})**
AuL12	-	9.0
AuL12/β-CD	1432	2.1
AuL12/Me-β-CD	380	7.9
AuL12/HP-β-CD	186	3.9

Table 1. Apparent stability constants (K_c) of AuL12/CD supramolecular complexes obtained by data processing of the solubility profiles associated with the co-solubilization (Method A) and degradation rate constants of the gold(III) complex and when encapsulated in different cyclodextrins.

3.1.3 *Drug degradation studies.*

The degradation profiles of AuL12 in 0.01 M phosphate buffer, 0.15 M NaCl, at pH 7.4 without or in the presence of β-CD, Me- β-CD and HP-β-CD, reported in Figure S5, showed in all cases that AuL12 undergoes first-order degradation kinetics. In physiologic buffer, the free drug undergoes rapid degradation while either natural or semisynthetic β-CDs improve the drug stability as shown in Table 1. The degradation rate constant obtained with β-CD was about 4 times lower than that obtained in plain buffer. Furthermore, β-CDs were the most efficient in preventing the AuL12 degradation, in agreement with the higher apparent stability constants compared to the other tested CDs. Unexpectedly, Me-β-CDs had only a negligible effect on the drug stability. Although the apparent stability constants of AuL12/Me-β-CD was higher than that calculated with AuL12/HP-β-CD, Me-β-CDs were less efficient in protecting AuL12 from degradation than HP-β-CD. According to the

evidence that HP-β-CDs are more efficient in preventing the AuL12 degradation and their high biocompatibility, which make them useful for clinical use even for parenteral administration, [54-55] the subsequent experiments were carried out with this type of nanocarriers.

3.2 Biological evaluation

3.2.1. Cytotoxicity Assays.

Cell viability studies were carried out by treating HeLa (human cervical carcinoma), KB (human nasopharyngeal epidermal carcinoma) and MCF7 (human breast adenocarcinoma) cells with different concentrations of AuL12 pre-dissolved in DMSO (AuL12/DMSO) or co-administered with HP-β-CD (AuL12/HP-β-CD) in a 1:5 molar ratio. The obtained cell viability profiles highlight that the co-administration with HP-β-CD preserves the AuL12 cytotoxic properties towards the HeLa cell line. The IC50 values were calculated (Table 2) and show that, against the KB and MCF7 cell lines, the activity of AuL12 / HP-β-CD system is about 30% higher than that of AuL12/DMSO.

	IC_{50} (μM)	
	AuL12/DMSO	**AuL12/HP-βCD**
HeLa	7.3 ± 0.8	7.5 ± 0.4
KB	30 ± 1	20.8 ± 0.9
MCF7	12.5 ± 0.6	9.3 ± 0.7

Table 2. IC_{50} values (μM) evaluated after 24-h treatment with the AuL12 complex pre-dissolved in DMSO or encapsulated in HP-βCD.

3.2.2 Pharmacokinetic studies.

According to the regulatory record of the investigated oligosaccharides and the suitable results obtained with HP-β-CD, namely high AuL12 solubility and stability, pharmacokinetic studies were carried out for the AuL12/HP-β-CD system. The formulation was intravenously injected into 8 mice and gold content in blood samples was detected at scheduled times. The pharmacokinetic profile of gold is reported in Figure S6. After 8 hours from injection, about 12% of the initial gold concentration could be detected in blood. The elaboration of the experimental data (by Kinetica Software) showed that AuL12 undergoes a bi-phasic behavior in the bloodstream ($C_t=Ae^{-\alpha t} + Be^{-\beta t}$), with a fast distribution to the peripheral compartment (α phase) followed by a slow elimination phase (β phase). The pharmacokinetic parameters reported in Table 3 highlight that the distribution phase is very fast with a $t\alpha_{1/2}$ of few minutes (7.4 min). The distribution volume at the steady state (V_{ss}) was about 3-fold higher than the central compartment volume (V_c), thus indicating that a moderate quantity of gold distributed in the peripheral compartment. The k_{12}/k_{21} ratio was 2.3 (k_{12} is the first-order transfer from central compartment (1) to peripheral compartment (2) and *vice versa*), pointing out the central-to-peripheral distribution was faster than the peripheral-to-central process. The slow elimination from the body ($t_{\beta 1/2}$ 14.28 h) and slow clearance from the blood (CL) reflected in high bioavailability (total drug amount that reaches the blood, $AUC_{0-\infty}$).

	AuL12/HP-β-CD
V_c (mL)	2.074
AUC $_{0\rightarrow\infty}$ (μg ml^{-1} h)	178.9
$t_{1/2\alpha}$ (h)	0.12
$t_{1/2\beta}$ (h)	14.28
V_{ss} (mL)	6.77
Cl (mL/h)	0.005597
k_e (h^{-1})	0.00269
k_{12} (h^{-1})	0.06319
k_{21} (h^{-1})	0.02791

Table 3. Main pharmacokinetic parameters obtained by data elaboration of the PK profiles of AuL12/HP-β-CD intravenously injected to mice. V_c, central compartment volume; AUC $_{0\rightarrow\infty}$, area under the curve; $t_{1/2\alpha}$ half-time of α-phase; $t_{1/2\beta}$, half-time of β-phase; Vss, distribution volume at the steady state; Cl, clearance; k_e, elimination rate constant; k_{12}, central compartment-to-peripheral compartment distribution rate constant; k_{21}, peripheral compartment-to-central compartment distribution rate constant.

These results are in good agreement with data reported in literature for the gold(I)-containing drugs aurothiomalate (GST) and auranofin (AF), used in immunosuppressive treatments as anti-rheumatic and antiarthritic drugs.[62-63] On the whole, few PK studies involved mice treated with AF or GST even though the results are often unclear.[63-65] In 1983, Walz and co-workers reported the PK of AF and GST after oral and parenteral administration to rats.[58] After oral administration AF displayed blood half-life of 28.8 h and the parenterally-administered GST showed a bi-phasic behavior.[56, 58-61]

In humans, in single-dose PK studies Blocka et al. found that peak plasma gold concentrations after oral administration of ^{195}Au-labelled AF (6 mg) solutions occurred at 1.2-2 hours.[21, 64, 70] Initial half-life was found to be 4 hours and terminal plasma half-lives ranged from 17 to 25 days but ^{195}Au was detectable in plasma for about 70-80 days.

[63, 64, 70] With respect to GST, following a 50-mg intramuscular injection, the serum gold concentration peaks at 2 to 6 hours.[62-63] If the single dose of ^{195}Au-containing GST is instead intravenously injected, the initial serum half-life was approximately 6 days and the terminal serum half-life ranges from 10 to 35 days.[70, 72-74]

3.2.3 AuL12 interferes upstream of the ubiquitin-proteasome pathway.

In previous works, some of us demonstrated that Au(III) dithiocarbamate complexes inhibit proteasome activity (purified enzyme and cell extracts).[36-38] However, it should be reminded that proteasomal degradation is initiated by the Ub-activating enzyme E1, which adenylates the C-terminus of ubiquitin (a Glycine residue - G76) in an ATP-dependent fashion to form a high-energy thioester bond by a cysteine residue. Then, E1 hands the activated Ub over to a conjugating enzyme (E2) to form an E2-Ub complex in proximity to the target protein. The final ubiquitination of the substrate occurs through the action of E3 ubiquitin ligases (Figure 2).[29-31, 75] As a result, different types of poly-Ub chains can be built up. For example, subsequent conjugations with K48-linked polyUb chains are associated with substrate targeting to the proteasome for degradation.[76-80] Therefore, in order to get further insight into the molecular mechanisms underlying the pro-apoptotic potential of AuL12, in this work we investigated whether AuL12 is also able to interfere with the upstream molecular events regulating the UPS. To this aim, polyubiquitination experiments were performed *in vitro* either in the presence or in the absence of AuL12. In particular, we tested Lys48-linked polyUb chain synthesis at increasing of AuL12

concentrations, from 0.5 to 7 µM (Figure 3). PolyUb chain synthesis was inhibited in a concentration-dependent manner, as evidenced by the decreased density of the blots corresponding to Ub_2, Ub_3, Ub_4 and Ub_5. The polyUb reaction was significantly inhibited even at a concentration of AuL12 of 0.5 µM and, remarkably, it was fully quenched at 7 µM. AuL12 may block Ub chain elongation at different levels of the polyubiquitination reactions. To address this issue, mixtures of Ub and E2-25K (the E2 enzyme that we used to catalyze the elongation of Lys48-linked polyUb chains) were co-incubated in the presence of increasing concentrations of AuL12 and analyzed by SDS-PAGE. SDS-PAGE of control AuL12-free mixtures of Ub/E2-25K (~ 33 kDa) shows a band corresponding to the Ub/E2 assembly (Supporting Information Figure S7, lane 3), ascribable to an interaction between the two proteins. SDS-PAGE of Ub/E2-25K mixtures incubated in the presence of increasing amounts of the gold(III) compound again shows this band (Supporting Information Figure S7, lanes 4-8) and demonstrates that AuL12 does not interfere in Ub/E2 interactions.

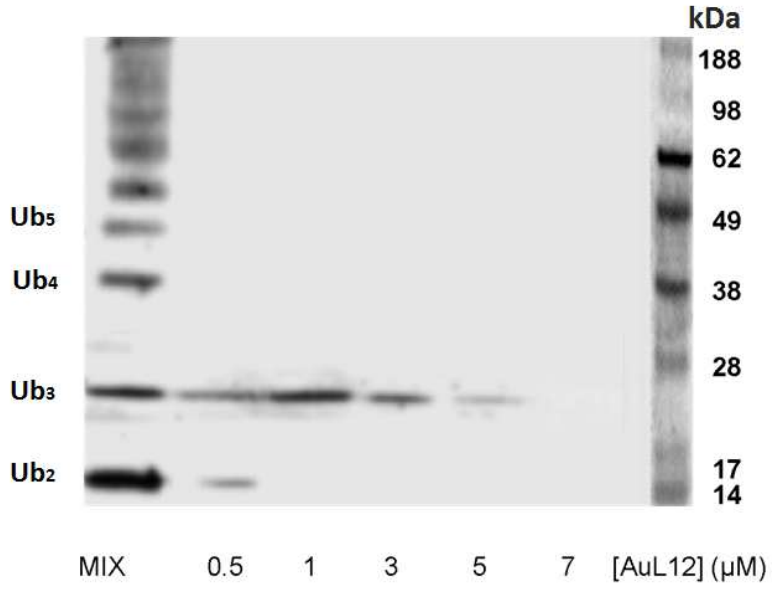

Figure 3. Lys-48 PolyUb chain synthesis carried out in the presence of increasing concentrations of AuL12 (0.5-7 μM). Assays and Western blotting were carried out as described in ESI (Ub MW *ca.* 8.5 kDa).

In order to verify whether AuL12 is able to inhibit Ub activation even more upstream of the Ub-conjugating machinery, we focused on the E1 enzyme. In fact, the ubiquitination process is initiated by ubiquitin activation where the E1 enzyme binds ATP-Mg^{2+} and ubiquitin, and catalyses the acyl adenylation of the ubiquitin C-terminus (Figure 2). Then, a cysteine of the E1 enzyme attacks the ubiquitin-AMP complex through acyl substitution, resulting in an Ub-E1 thioester bond and simultaneous AMP releasing.[81-82] Therefore, the E1-Ub covalent complex should be visible if Ub activation works properly. We have incubated E1, ATP, Mg^{2+} and Ub with 3 and 5 μM AuL12 (Figure 4, lanes 4 and 5). Contrary to control experiments, performed in the absence of AuL12 (Figure 4, lane 3), the presence of AuL12 hinders the formation of the E1-Ub adduct. This means that AuL12 inhibits Ub activation and, consequently, Ub conjugation and downstream signaling. This was further proved by incubating the samples also in the presence of the Ub-conjugating E2 enzyme. In fact, contrary to lane 2 (control), when the tested gold(III) compound is added (lane 1) polyUb species are not formed. This confirms the upstream effect of AuL12 at the E1 level (lane 5) of the overall pathway.

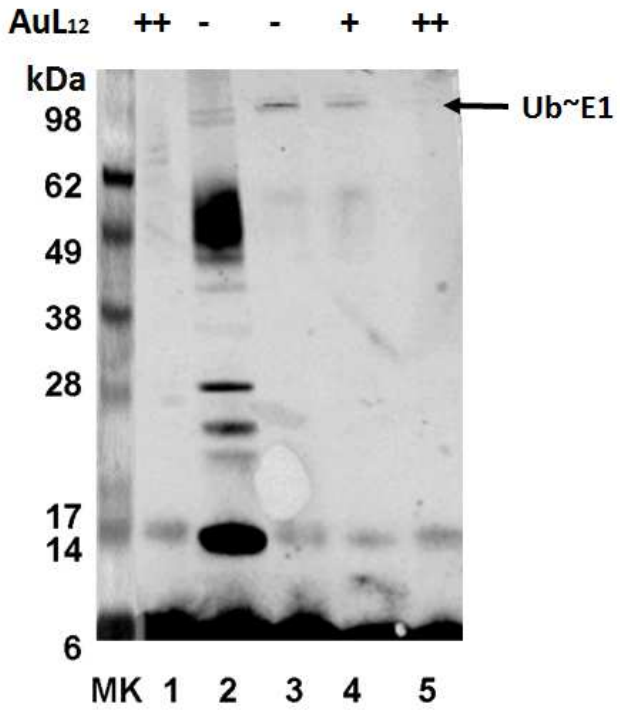

Figure 4. Effects of AuL12 on the Ubiquitin adenylate formation. Lane 1: Ub (50 μM), E1 (0.5 μM), E2-25K (1 μM), AuL12 (5 μM); lane 2: Ub (50 μM), E1 (0.5 μM), E2-25K (1 μM); lane 3: E1 (2.5 μM), Ub (50μM); lane 4-5: E1 (2.5 μM), Ub (50μM), in the presence of AuL12, respectively 3 and 5 μM (Ub MW *ca.* 8.5 kDa).

To further study the role of AuL12 in inhibiting Ub activation, MALDI-TOF-MS measurements were carried out. In particular, the aim of these measurements was to clarify the ability of this compound to prevent E1-Ub complex formation when added into the Mg^{2+}-ATP reaction mixture. MALDI-TOF MS measurements were performed using SIN as a matrix and the "dried-droplet" as sample preparation method (see Supporting Information). It should be pointed out that some limitations, in terms of signal intensity and resolution, can be encountered in detecting high molecular-weight proteins by using MALDI-TOF-MS instruments equipped with conventional microchannel plate (MCP) detectors.[83] As a matter of fact, the MALDI-MS spectrum recorded for the ubiquitin-activating enzyme (E1)

is characterized by low intensity signals attributed to the mono- and double-charge E1 species at about m/z 60,000 and 120,000, respectively (Supporting Information Figure S8A). Although the low signal-to-noise ratio observed in the former mass spectrum, the comparison with the spectrum recorded when the ubiquitin-activating reaction occurs (Supporting Information Figure S8B), points out the appearance of a shoulder at higher m/z values, ascribable to the E1-Ub complex formation. Despite MALDI is a sensitive ionization technique, high concentrations of buffers and other contaminants may interfere with the desorption and ionization process of the analyte. Therefore, in order to enhance the signal intensity, several experimental conditions were tested. In particular, when the reagents for the ubiquitin-activating reaction (IPP, DTT, Mg^{2+}-ATP) were not added to the E1/Ub sample solution, more defined signals were observed (Supporting Information Figure S9A and S9B). These experimental conditions did not allow the formation of the E1- ubiquitin thioester bond, thus highlighting the observed E1-Ub complex just involves supramolecular interactions. These findings point out our MALDI-MS final conditions are able to detect the E1- Ub non-covalent adduct. In this context, the capacity of MALDI-TOFMS to detect intact non-covalent biomolecular complexes, has been demonstrated in other works.[84-86] It must be mentioned that a quite high number of interacting partners (10-30 picomole/µL) might favor the formation of nonspecific protein-protein complexes or aggregates. Nevertheless, the lower analyte concentration used in our experiments (1-2.5 picomole/µL) might preserve, at least partially, the interaction occurring in solution and minimize the formation of nonspecific interactions in the gas phase, as reported recently in literature.[87]Interestingly, the mass spectrum recorded after addition of AuL12 to the sample containing the E1/Ub mixture, showed a clear reduction of the signal intensity

corresponding to the E1-Ub adduct (Figure S9C). This behavior suggests the inhibitory effect of AuL12 could occur at the adenylation domain of E1, where Ub/E1 non-covalent interactions take place.[88]

3.2.4 AuL12 inhibits proteasome activity in living intact cells.

In the first part of the paper, we described the growth-inhibitory effects of AuL12 toward three human tumor cell lines by an MTT assay over 24-h incubation. Among the tested cell lines, we chose the breast cancer MCF7 cell line to evaluate the possible proteasome-inhibitory activity of AuL12 after 6-h treatment. First, we tested the ability of AuL12 to inhibit cell proliferation in a short-time incubation, finding a dose-dependent behavior (Figure 5A). It is worth noting that at the lowest tested concentration (0.5 μM), the gold(III) compound turned out to be non-cytotoxic. Likewise, bortezomib, a clinically-established

proteasome inhibitor, here used as a control (1 µM), did not inhibit cell growth under the same conditions.

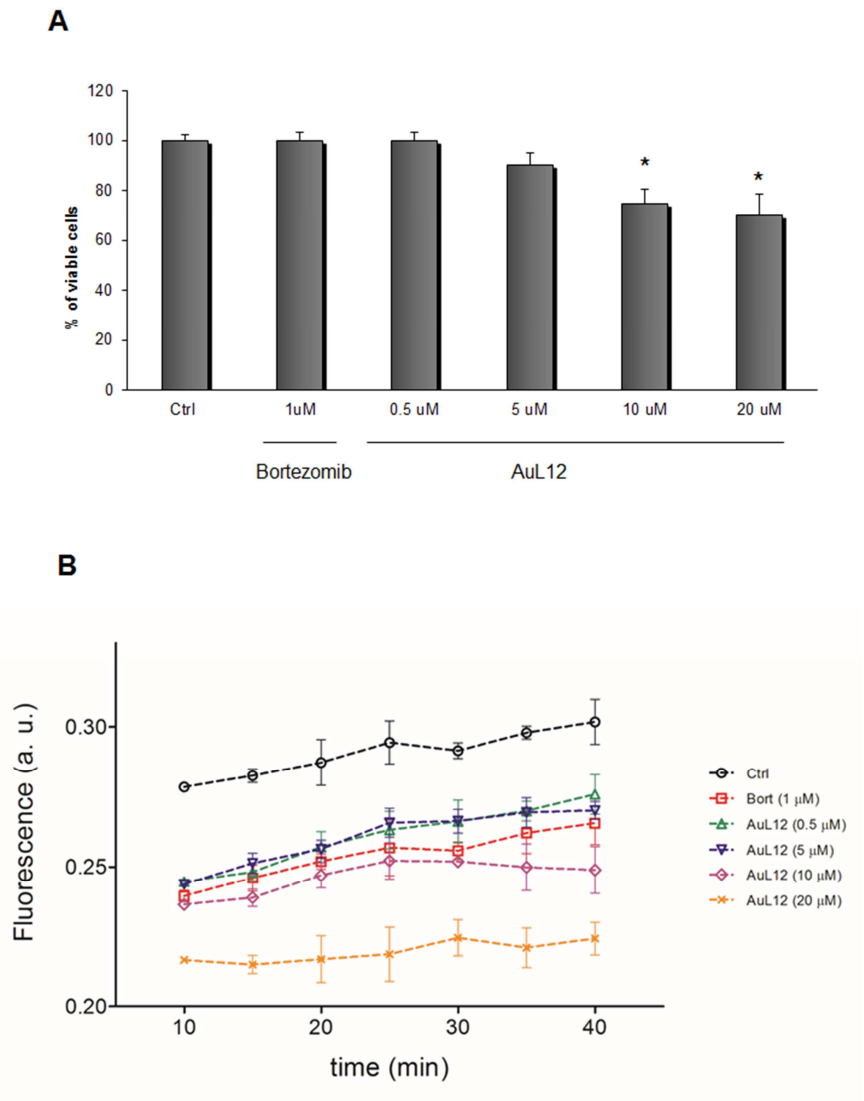

Figure 5. The investigated gold(III) compound AuL12 inhibits the proliferation of MCF7 cells and the activity of proteasome in living intact cells. A: Dose-dependent loss of mitochondrial (MTT) activity in MCF7 cells treated with 0.5 to 20 µM of AuL12 for 6 hours at 37 °C. Changes in reductase activity are expressed in percentage referred to the control (DMSO). Each value represents the mean ± SD of five independent experiments. A significant difference from control value is indicated by * ($p<0.05$) (one-way ANOVA with Tukey's post-hoc test). B: Inhibition of the chymotrypsin-like activity of proteasome over time in intact living cells in the presence of bortezomib and AuL12 at the indicated concentrations, using DMSO as a control. The

reported values refer to the whole cell population and are obtained by monitoring the fluorescence of the TED probe on a plate reader as described in Supporting Information.

To investigate whether AuL12 could inhibit proteasomal activity in living cells, MCF7 cells were treated for 6 hours with 0.5-20 µM AuL12 or with 1 µM bortezomib. Then, cell cultures were incubated in the presence of the TED reporter (50 µM) (see Supporting Information). TED (TAT-EDANS-DABCYL) is an engineered internally quenched fluorogenic peptide with a proteasome-specific cleavage motif fused to a TAT (Transactivator of Transcription) moiety and linked to the fluorophores DABCYL (4-(4-dimethylaminophenylazo)benzoic acid) and EDANS (5-(2- aminoethyl)amino]naphthalene-1-sulfonic acid).[42] This peptide penetrates cell membranes and is rapidly cleaved by the proteasomal chymotrypsin-like activity, generating a quantitative fluorescent probe for proteasome activity investigations in living cells. [42] Therefore, the effect of AuL12 on the proteasomal chymotrypsin-like activity was assessed by fluorescence analysis carried out over time by using the bottom reading mode of the Varioskan microplate reader. DMSO was used to pre-dissolve the gold(III) compound and hence taken as a negative control in all our experiments. AuL12 significantly inhibited proteasomal chymotrypsin-like activity in MCF7 cells at all concentrations after 6-h treatment (Figure 5B). Interestingly, at the lowest tested concentration (0.5 µM) AuL12, although not cytotoxic, was effective in inhibiting the proteasomal activity as measured by TED fluorescence emission. The reduction of TED fluorescence emission by AuL12 was also followed over time at single cell level by confocal microscopy. Considering the data obtained with 5 µM AuL12, both on cell viability and on proteasome inhibition, we exploited this concentration in time lapse experiments. Images reported in Figure 6A clearly show the increase of the TED fluorescence emission due to the

peptide cleavage by the active proteasome in non-treated cells. Pre-incubation for 6 h with 5 µM AuL12 significantly prevented the TED fluorescence from increasing as also observed for Bortezomib (Figure 5A and 6B). Taken together, these experiments point out that AuL12 targets UPS not only in cell-free systems (the purified 20S proteasome and cell extracts)[36-38] but also in intact cells.

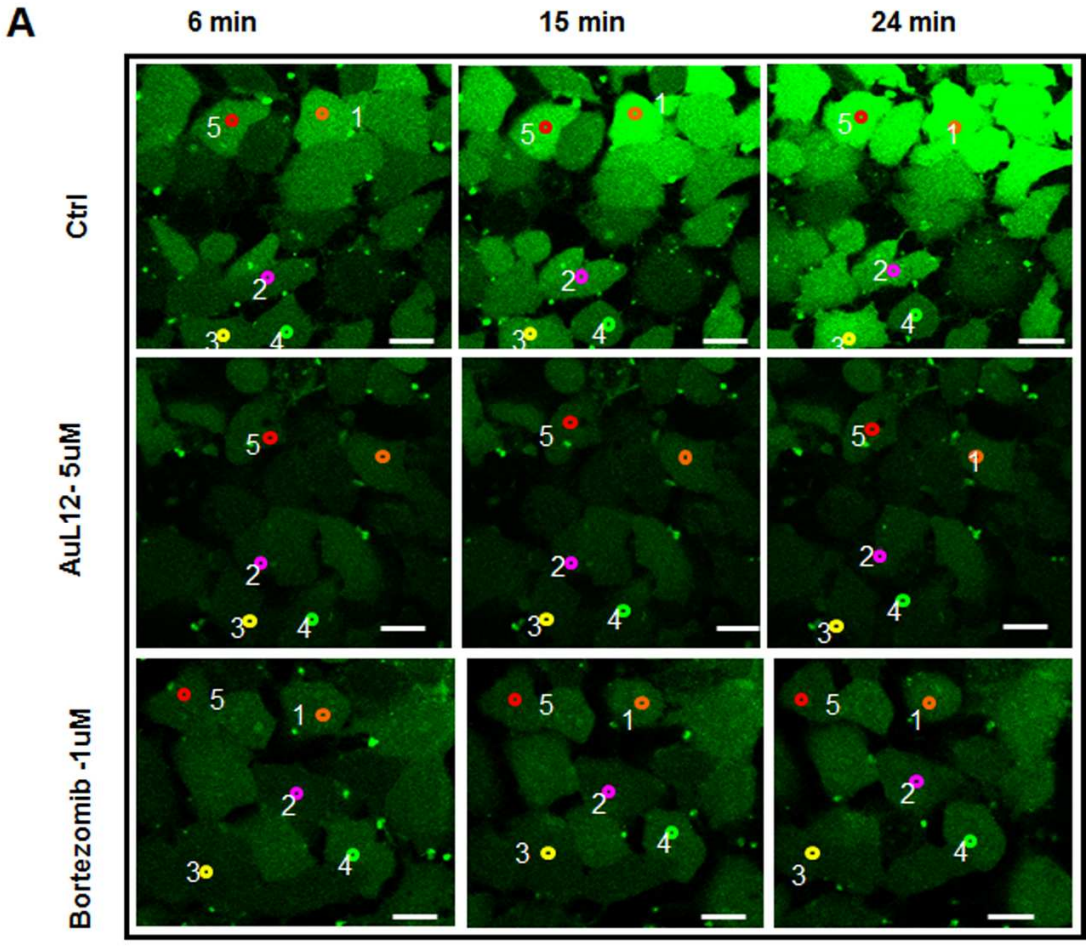
A
6 min
15 min
24 min
Ctrl
AuL12- 5uM
Bortezomib -1uM
B
Fluorescence (au)
time (min)
Ctrl
AuL12-5µM
Bortezomib- 1µM
0
5
10
15
20
25
30
35
40
45
1
3
6
9
12
15
18
21
24

Figure 6. AuL12 inhibits the chymotrypsin-like activity of proteasome over time in single intact living cells. Measurements were made on single cells pre-incubated with AuL12 or bortezomib at 5 and 1 μM, respectively, with DMSO as a control. The proteasome activity was determined by following the fluorescence emission of the TED probe by confocal microscopy as described in Supporting Information. (A), representative images of time lapse incubations with 50 μM TED, being analyzed by drawing regions inside individual cells and measuring the mean fluorescence value as shown in the chart (panel B). For each condition the reported values represent the mean fluorescence intensity measured inside all the shown cells corrected for the basal fluorescence.

3.2.5 AuL12 uptake is rapid and energy-dependent.

The mechanism by which AuL12 prompts tumor cell death has been largely characterized. [5] However, it has not been clearly understood yet how the compound reaches its targets inside the cell. Here, we have used simple experimental strategies to get further insight on the matter. The effect of AuL12 on cell proliferation as well as chymotrypsin-like activity of proteasome, was assessed by exposing MCF7 cells, kept at 4 °C for 60 minutes, to increasing concentrations of AuL12 (0.5-20 μM). In these conditions, where the endocytosis and other energy-dependent uptake processes are inhibited, AuL12 affected neither cell growth (Figure 7A) nor proteasome activity (Figure 7B). Likewise, 1 μM bortezomib was not able to inhibit the proteasome activity when incubated with cells at 4°C. The hypothesis of an energy-dependent uptake was experimentally tested also by assessing the effects of AuL12 and bortezomib on MCF7 cells in the presence of cytochalasin, a well-known inhibitor of endocytosis. Cells were pre-incubated for 1h in the presence of cytochalasin before being exposed to increasing concentrations of AuL12 (0.5-20 μM) for 6 hours at 37 °C. Bortezomib was again used as a control. We found that after cytochalasin treatment, the effects of AuL12 and Bortezomib on both cell death induction and proteasome inhibition

were abolished (Supporting Information Figure S10). Thus, our findings suggest that AuL12 enters cells by an energy-dependent process.

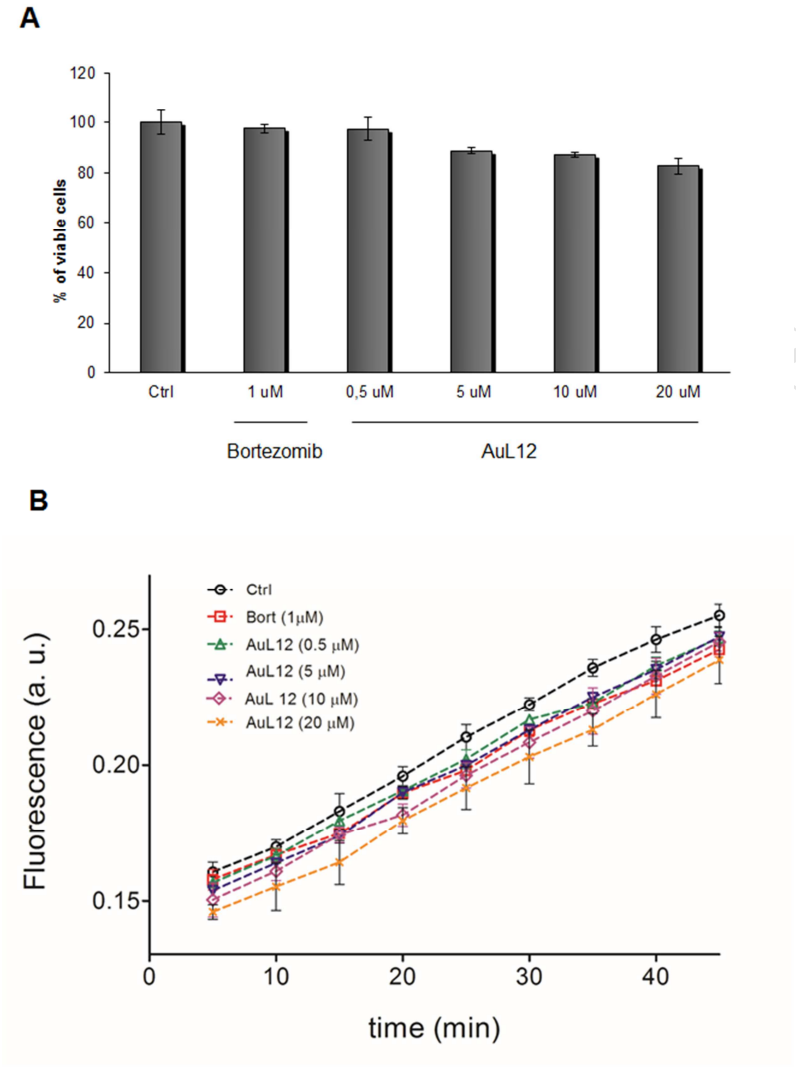

Figure 7. AuL12 enters MCF7 cells *via* an energy-dependent mechanism. A: Loss of mitochondrial (MTT) activity in MCF7 cells exposed to 0.5-20 µM of AuL12 or 1 µM Bortezomib at 4°C (60 min). Change in reductase activity was measured after 5 hours incubation at 37°C in the absence of AuL12 and/or Bortezomib. Cell viability is expressed as the percentage referred to the control (DMSO). Each value represents the mean ± SD of five independent experiments. B: Inhibition of the proteasomal chymotrypsin-like activity over time in intact living cells. Cells were exposed to 0.5-20 µM AuL12 or 1 µM Bortezomib at 4°C for 60 minutes

followed by 5 hours incubation at 37°C in the absence of AuL12 and/or Bortezomib. DMSO was used as a control.

4. Conclusions

Cisplatin is a well-known antineoplastic drug used alone or in combination therapy for the treatment of many cancers. Although being among the most marketed anticancer drugs worldwide, [89] its poor toxicological profile somehow limits the clinical use. So far, several cisplatin analogues and other metal-based derivatives have been studied.[90-93] Among them, our gold(III)-dithiocarbamate complexes possess interesting antitumor activity and low or no toxicity.[4-5] In this work, we have increased the stability, the water solubility and bioavailability of our model compound AuL12 by preparing and testing supramolecular complexes with the natural oligosaccharides β–cyclodextrins, endowed with a cavity volume of ca. 260 Å[3]. In particular, the HP-β-CD proved able to protect the AuL12 compound from degradation in phosphate buffer, used to mimic physiological conditions. In light of the obtained PK profile, the unique mechanism of action and the confirmed antitumor activity of the test compound, we have planned future in-depth studies on the reactivity of AuL12 under physiological conditions and towards biomolecules (*e.g.*, human serum albumin, DNA and ascorbate) along with metabolism investigations in terms of redox chemistry, starting from the data reported for the gold(I)-based reference drugs.[94-95] With respect to the mechanism of action, we focused on the carefully orchestrated ubiquitin-proteasome pathway, based on the covalent binding of one or more ubiquitin molecules (Ub) to target proteins, ultimately leading to their subsequent intracellular degradation. Inhibitors of such a system may affect either directly the 20S proteasome catalytic core or can play a key role in

unbalancing upstream events (*e.g.*, ubiquitin chain growth), thus anyway altering the proteasome functionality.[95-96] Contrary to the proteasome, Ub-activating and -conjugating enzymes are substrate-specific. Therefore, the discovery of new compounds able to inhibit only or mainly the latter, compared to the former, may lead to the development of innovative drugs with fewer side effects. Remarkably, AuL12 i) inhibits Lys48 self-polyubiquitination reactions, ii) does not interfere with Ub-E2 interactions but iii) thwarts the Ub activation by E1. In this context, it is worth highlighting that even when the E1-ubiquitin thioester was not formed, our MALDI-MS measurements were able to identify the noncovalent adduct E1-Ub. We found also that AuL12 inhibits proteasome in cell with a potency similar to that of bortezomib and that a concentration of 7 µM was also able to completely block ubiquitin chain growth under cell-free conditions. Finally, our experiments point out that the AuL12 mechanism of action relies on an energy-dependent uptake. This was stated again by exploiting the cytochalasin endocytosis inhibitor.

AUTHOR INFORMATION

Corresponding Author

*E-mail: dolores.fregona@unipd.it; giuseppe.pappalardo@cnr.it

Author Contributions

# M.F.T. and C.N. contributed equally to this work.

Notes

The authors declare no competing financial interest.

ACKNOWLEDGMENT

This work was financially supported by PRIN2009 Prot. 2009_WCNS5C, PRAT2015, Progetto Strategico di Ateneo 2011 “Nanochemistry and medicine for cancer: from diagnosis to treatment (NAMECA)” and A.R.TE.M.O. Association (Italy). N.P.’s PhD fellowship is granted by T.R.N. IMBALLAGGI – logistic services (www.trnimballaggi.it/en/).

ABBREVIATIONS

β-CD, beta-cyclodextrin; ACN, acetonitrile; AMP, adenosine monophosphate; ATP, adenosine triphosphate; CCK8, cholecystokinin octapeptide; CD, cyclodextrin; DABCYL, (4-(4-dimethylaminophenylazo) benzoic acid); DMSO, dimethyl sulphoxide; DSPE-PEG, poly(ethylene glycol)-distearoylphosphatidylethanolamine; DTT, Dithiothreitol; DUBs, deubiquitinase enzymes; EDANS, 5-(2- aminoethyl)amino]naphthalene-1-sulfonic acid; FDA, Food and Drug Administration; HP-β-CD, (2-hydroxylpropyl)-beta-cyclodextrin; IPP, inorganic pyrophophatase; Me-β-CD, beta-cyclodextrin methyl ethers; MTT, 3-(4,5-dimethylthiazol-2-yl)-2,5-diphenyltetrazolium bromide; Poly-Ub, poly-ubiquitinylated; SDS-Page, sodium dodecyl sulphate - polyacrylamide gel electrophoresis; TED, internally quenched fluorogenic

peptide, TAT-EDANS-DABCYL; TFA, Trifluoroacetic acid; TRIS, Tris(Hydroxymethyl)aminomethane; Ub, ubiquitin; UPS, ubiquitine-proteasome system.

REFERENCES

1. L. Kelland, The resurgence of platinum-based cancer chemotherapy. Nat. Rev. Cancer, 7 (2007) 573-584.
2. A. M. Florea, D. Büsselberg, Cisplatin as an anti-tumor drug: cellular mechanisms of activity, drug resistance and induced side effects. Cancers 3 (2011) 1351-1371.
3. H.S. Oberoi, N.V. Nukolova, A.V. Kabanov, T.K. Bronich, Nanocarriers for delivery of platinum anticancer drugs. Adv. Drug Deliv. Rev. 65 (2013) 1667-1685.
4. C. Nardon, G. Boscutti,; D. Fregona, Beyond platinums: gold complexes as anticancer agents. Anticancer Res. 34 (2014) 487-492.
5. C. Nardon, D. Fregona, Gold(III) complexes in the oncological preclinical arena: from aminoderivatives to peptidomimetics. Curr. Top. Med. Chem. 16 (2016) 360-380.
6. L. Ronconi, C. Marzano, P. Zanello, M. Corsini,; G. Miolo,; Maccà, C.; Trevisan A.; Fregona, D. Gold(III) dithiocarbamate derivatives for the treatment of cancer: solution chemistry, DNA binding, and hemolytic properties. J. Med. Chem. 49 (2006) 1648-1657.
7. P. Ringhieri, R. Iannitti, C. Nardon, R. Palumbo, D. Fregona, G. Morelli, A. Accardo Target selective micelles for bombesin receptors incorporating Au(III)-dithiocarbamato complexes. Int. J. Pharm. 473 (2014) 194-202.

8. C. Nardon, G. Boscutti, L. Dalla Via, V. Di Noto, G. Morelli, A. Accardo, D. Fregona, CCK8 peptide-labeled Pluronic® F127 micelles as a targeted vehicle of gold-based anticancer chemotherapeutics. MedChemComm. 6 (2015) 155-163.
9. G. Crini A History of Cyclodextrins. Chem. Rev. 114 (2014) 10940-10975.
10. Q. D. Hu, G. P. Tang, P. K. Chu, Cyclodextrin-based host-guest supramolecular nanoparticles for delivery: from design to applications. Acc. Chem. Res. 47 (2014) 2017-2025.
11. M. V. Ol'khovich, A. V. Sharapova, S. N. Lavrenov, S. V. Blokhina, G. L. Perlovich, Inclusion complexes of hydroxypropyl-β-cyclodextrin with novel cytotoxic compounds: solubility and thermodynamic properties. Fluid Phase Equilib. 384 (2014) 68-72.
12. V. B. Jadhav, Y. J. Jun, J. H. Song, M. K. Park, J. H. Oh, S. W. Chae, I. S. Kim, S. J. Choi, H. J. Le, Y. S. Sohn, A novel micelle-encapsulated platinum(II) anticancer agent. J. Control. Release 147 (2010) 144-150.
13. P. J. Avaji, H. I. Joo, J. H. Park, K. S. Park, Y. J. Junc, H. J. Lee, Y. S. Sohn, Synthesis and properties of a new micellar polyphosphazene–platinum(II) conjugate drug. J. Inorg. Biochem. 140 (2014) 45-52.
14. T. Watanabe, H. Monzen, M. Hara, T. Mizowaki, M. Hiraoka Pharmacokinetic model of myocardial (99m)Tc-sestamibi washout. Ann. Nucl. Med. 27 (2013) 279-284.
15. Y. Li, P. Guo, N. Lin, Q. Li, Pharmacokinetics of di-phenyl-di-(2,4-dichlorbenzohydroxamato) tin (IV): A new metal-based candidate with promising antitumor activity in rats. Inorg. Chim. Acta 423 (2014) 235-241.

16. Y. Wu, L. Ding, N.Y. Huang, A.D. Wen, B. Liu, W. B. Li, Pharmacokinetics of metronidazole, tetracycline and bismuth in healthy volunteers after oral administration of compound tablets containing a combination of metronidazole, tetracycline hydrochloride and bismuth oxide. Drug Res. 65 (2015) 74-78.
17. I. Ott, Biodistribution of Metals and Metallodrugs. In: J. Reedijk, K. Poeppelmeier Comprehensive inorganic chemistry II: from elements to applications, 2nd ed.; Eds.; Elsevier: Amsterdam, 2013, Vol. 3 933-949.
18. G. Vértiz, L. E. García-Ortuño, J. P. Bernal, M. E. Bravo-Gómez, E. Lounejeva, A. Huerta, L. Ruiz-Azuara, Pharmacokinetics and hematotoxicity of a novel copper-based anticancer agent: casiopeina III-Ea, after a single intravenous dose in rats. Fundam. Clin. Pharmacol. 28 (2014) 78-87.
19. C. Sessa, G. Capri, L. Gianni, F. Peccatori, G. Grasselli, J. Bauer, M. Zucchetti, L.Vigano, A. Gatti, C. Minoia, P. Liati, S. Van den Bosch, A. Bernareggi, G. Camboni, S. Marsoni, Clinical and pharmacological phase I study with accelerated titration design of a daily times five schedule of BBR3464, a novel cationic triplatinum complex. Ann. Oncol. 11 (2000) 977-983.
20. N. L. Gottlieb, Comparative pharmacokinetics of parenteral and oral gold compounds. J. Rheumatol. 8 (1982) 99-109.
21. K. Blocka, D. E. Furst, E. Landaw, S. Dromgoole, A. Blomberg, H. E.Paulus Single dose pharmacokinetics of auranofin in rheumatoid arthritis. J. Rheumatol. 8 (1982) 110-119.

22. T. A. Grigoreva, V. G. Tribulovich, A. V. Garabadzhiu, G. Melino, N. A.Barlev The 26S proteasome is a multifaceted target for anti-cancer therapies. Oncotarget 6 (2015) 24733-24749.

23. D. E. Johnson, The ubiquitin-proteasome system: opportunities for therapeutic intervention in solid tumors Endocr.-relat. cancer 22 (2015) T1-T17.

24. L. Dalla Via, C. Nardon, D. Fregona Targeting the ubiquitin–proteasome pathway with inorganic compounds to fight cancer: a challenge for the future. Future Med. Chem. 4 (2012) 525-543.

25. A. F. Kisselev, W. A. Van Der Linden, H. S. Overkleeft, Proteasome inhibitors: an expanding army attacking a unique target. Chem. Biol. 19 (2012) 99-115.

26. A. McBride, J. O. Klaus, K. Stockerl-Goldstein, Carfilzomib: a second-generation proteasome inhibitor for the treatment of multiple myeloma. Am. J. Health Syst. Pharm. 72 (2015) 353-360.

27. A.M. Santoro, M. C. Lo Giudice, A. D'Urso, R. Lauceri, Purrello, R.; Milardi, D. Cationic porphyrins are reversible proteasome inhibitors. J. Am. Chem. Soc. 134 (2012) 10451-10457.

28. A. M. Santoro, A. Cunsolo, A. D'Urso, D. Sbardella, G. R. Tundo, C. Ciaccio, M. Coletta, D. Diana, R. Fattorusso, M. Persico, A. Di Dato, C. Fattorusso, D. Milardi, R. Purrello, Cationic porphyrins are tunable gatekeepers of the 20S proteasome. Chem. Sci. 7 (2016) 1286-1297.

29. L. Borissenko, M. Groll, 20S proteasome and its inhibitors: crystallographic knowledge for drug development. Chem. Rev. 107 (2007) 687-717

30. R.J. Deshaies, Protein degradation: Prime time for PROTACs, Nat. Chem. Biol. 11 (2015) 634–635.

31. A. Ciechanover, Proteolysis: from the lysosome to ubiquitin and the proteasome. Nat. Rev. Mol. Cell. Biol. 16 (2015) 322-324.

32. Y.C. Hou, J.Y. Deng. Role of E3 ubiquitin ligases in gastric cancer. World J. Gastroenterol. 21 (2015) 786-93.

33. H. An, and A. V. Statsyuk, An inhibitor of ubiquitin conjugation and aggresome formation. Chem. Sci. 6 (2015) 5235-5245.

34. Y. Yang, J. Kitagaki, R. M. Dai, Y. C Tsai, K. L. Lorick, R. L. Ludwig, S. A. Pierre, J. P. Jensen, I. V. Davydov, P. Oberoi, C. C. Li, J. H. Kenten, J. A. Beutler, K. H. Vousden, A. M. Weissman Inhibitors of ubiquitin-activating enzyme (E1), a new class of potential cancer therapeutics. Cancer Res. 67 (2007) 9472-9481.

35. G. Wei Xu, M. Ali, T. E. Wood, D. Wong, N. Maclean, X. Wang, M. Gronda, M. Skrtic, X. Li, R. Hurren, X. Mao, M. Venkatesan, R. B. Zavareh, T. Ketela, J. C. Reed, D. Rose, J. Moffat, R. A. Batey, S. Dhe-Paganon, A. D. Schimmer, The ubiquitin-activating enzyme E1 as a therapeutic target for the treatment of leukemia and multiple myeloma. Blood 115 (2010) 2251-2259

36. X. Zhang, M. Frezza, V. Milacic, L. Ronconi, Y. Fan, C. Bi, D. Fregona, Q. P. Dou, Inhibition of Tumor Proteasome Activity by Gold Dithiocarbamato Complexes via both Redox-Dependent and –Independent Processes J. Cell. Biochem. 109 (2010) 162-172.

37. V. Milacic, D. Chen, L. Ronconi, K. R. Landis-Piwowar, D. Fregona, Q.P. Dou, A novel anticancer gold(III) dithiocarbamate compound inhibits the activity of a purified

20S proteasome and 26S proteasome in human breast cancer cell cultures and xenografts. Cancer Res. 66 (2006) 10478-10486.

38. C. Nardon, S. M. Schmitt, H. Yang, J. Zuo, D. Fregona, Q. P. Dou, Gold(III)-Dithiocarbamato peptidomimetics in the forefront of the targeted anticancer therapy: preclinical studies against human breast neoplasia. PLoS One 9 (2014) e84248.
39. N. P. Dantuma, K. Lindsten, R. Glas, M. Jelne, M. G. Masucci, Short-lived green fluorescent proteins for quantifying ubiquitin/proteasome-dependent proteolysis in living cells. Nat. Biotecnol. 18 (2000) 538-43.
40. L. Rickardson, M. Wickstrom, R. Larsson, H. Lovborg Image-based screening for the identification of novel proteasome inhibitors. J. Biomol. Screen. 12 (2007) 203-210.
41. I. Momose, D. Tatsuda, S. Ohba, T. Masuda, D. Ikedaq, A. Nomoto In vivo imaging of proteasome inhibition using a proteasome-sensitive fluorescent reporter. Cancer Sci. 103 (2012) 1730-1736.
42. S. A. M. Urru, P. Veglianese, A. De Luigi, E. Fumagalli, E. Erba, R. Gonella-Diaza, A. Carrà, E. Davoli, T. Borsello, G. Forloni, N. Pengo, E. Monzani, P. Cascio, S. Cenci, R. Sitia, M. Salmona, A new fluorogenic peptide determines proteasome activity in single cells. J. Med Chem. 53 (2010) 7452-60.
43. G. Arena, R. Fattorusso, G. Grasso, G. I. Grasso, C. Isernia, G. Malgieri, D. Milardi, E. Rizzarelli Zinc(II) complexes of ubiquitin: speciation, affinity and binding features. Chem. Eur. J. 17 (2011) 11596-11603.
44. D. Milardi, F. Arnesano, G. Grasso, A. Magrì, G. Tabbì, S. Scintilla, G. Natile, E. Rizzarelli Ubiquitin stability and the Lys63-linked polyubiquitination site are compromised on copper binding. Angew. Chem. Int. Ed. 46 (2007) 7993-7995.

45. L. Ronconi, L. Giovagnini, C. Marzano, F. Bettìo, R. Graziani, G. Pilloni, D. Fregona Gold dithiocarbamate derivatives as potential antineoplastic agents: design, spectroscopic properties, and in vitro antitumor activity. Inorg. Chem. 44 (2005) 1867-1881.

46. T. J. Mosmann Rapid colorimetric assay for cellular growth and survival: application to proliferation and cytotoxicity assays. J. Immunol. Methods 65 (1983) 55 -63.

47. G. Grasso, V. Lanza, G. Malgieri, R. Fattorusso, A. Pietropaolo, E. Rizzarelli, D. Milardi The insulin degrading enzyme activates ubiquitin and promotes the formation of K48 and K63 diubiquitin. Chem. Comm. 51 (2015) 15724-15727.

48. J. J. Chen, C. A. Tsu, J. M. Gavin, M. A. Milhollen, F. J. Bruzzese, W. D. Mallender, M. D. Sintchak, N. J. Bump, X. Yang, J. Ma, H. Loke, Q. Xu, P. Li, N. F. Bence, J. E. Brownell, L. R. Dick Mechanistic studies of substrate-assisted inhibition of ubiquitin-activating enzyme by adenosine sulfamate analogues. J. Biol. Chem. 286 (2011) 40687-40877.

49. G. Arena, F. Bellia, G. Frasca, G. Grasso, V. Lanza, E. Rizzarelli, G. Tabbì, V. Zito, D. Milardi Inorganic stressors of ubiquitin. Inorg. Chem. 52 (2013) 9567-9573.

50. O. Yanes, F. X. Aviles, P. Roepstorff, T. J. D. Jørgensen Exploring the “intensity fading” phenomenon in the study of noncovalent interactions by MALDI-TOF mass spectrometry. J. Am. Soc. Mass Spectrom. 18 (2007) 359-367.

51. L. Ronconi, C. Nardon, G. Boscutti, D. Fregona, Perspective gold(III)-dithiocarbamato anticancer therapeutics: learning from the past, moving to the future. In: M. Prudhomme , Advances in Anti-Cancer Agents in Medicinal Chemistry; Ed.; Bentham e-book, Vol. 2, 2013, pp. 130-172.

52. European Medicines Agency: EMA/CHMP/333892/2013 - Background review for cyclodextrins used as excipients. April 2016.

53. T. Irie, K. Uekama, Pharmaceutical applications of cyclodextrins. III. Toxicological issues and safety evaluation. J. Pharm. Sci. 86 (1997) 147-162.

54. S. Gould, R. C. Scott, 2-Hydroxypropyl-beta-cyclodextrin (HP-beta-CD): a toxicology review. Food Chem. Toxicol. 43 (2005) 1451-1459.

55. V. J. Stella, H. Quanren Cyclodextrins. Toxicol. Pathol. 36 (2008) 30-42.

56. E. M. Martin Del Valle, Cyclodextrins and their uses: a review. Process Biochem. 39 (2004)1033-1046.

57. T. Higuchi, K. A. Connors Solid dispersion incorporated microcapsules: predictive tools for improve the half -life and dissolution rate of pioglitazone hydrochloride. Adv. Anal. Chem. Instrum. 4 (1965) 117-212.

58. R. Challa, A. Ahuja, J. Ali, R. K. Khar, Cyclodextrins in drug delivery: an updated review. AAPS PharmSciTech. 6 (2005) E329-E357.

59. L. Trollope, D. L. Cruickshank, T. Noonan, S. A. Bourne, M. Sorrenti, L. Catenacci, M. R. Caira Inclusion of trans-resveratrol in methylated cyclodextrins: synthesis and solid-state structures. Beilstein J. Org. Chem. 10 (2014) 3136–3151.

60. S. N. Hiremath, R. K. Raghavendra, F. Sunil, L. S. Danki, M. V. Rampure, P. V. Swamy, U.V. Bhosale Dissolution enhancement of gliclazide by preparation of inclusion complexes with β-cyclodextrin. Asia J. Pharm. 2 (2008) 73-76.

61. P. Bertholet, M. Gueders, G. Dive, A. Albert, V. Barillaro, B. Perly, D. Cataldo, G. Piel, L. Delattre, B. Evrard. The effect of cyclodextrins on the aqueous solubility of a new MMP inhibitor: phase solubility, ^{1}H-NMR spectroscopy and molecular modeling

studies, preparation and stability study of nebulizable solution. J. Pharm. Pharm. Sci. 8 (2005) 164-175.

62. F.C Shaw III C. Gold-based therapeutic agents. Chem. Rev. 99 (1999) 2589-2600.
63. L. Messori, G. Marcon Gold complexes in the treatment of rheumatoid arthritis. In: A. Sigel, Sigel H., Eds.; Marcel Dekker Metal Ions in Biological Systems; New York, Vol. 41, 2004, pp. 279-304.
64. D.E. Furst, Mechanism of action, pharmacology, clinical efficacy and side effects of auranofin. An orally administered organic gold compound for the treatment of rheumatoid arthritis. Pharmacother. 3 (1983) 284-298.
65. K. L. Blocka, Auranofin versus injectable gold. Comparison of pharmacokinetic properties. Am. J. Med. 75 (1983) 114-122.
66. D.T. Walz, M.J. Di Martino, D. E. Griswold, A. P. Intoccia, T. L. Flanagan Biologic actions and pharmacokinetic studies of auranofin. Am. J. Med. 75 (1983) 90-108.
67. A. P. Intoccia, T. L. Flanagan, D. T. Walz, L. Gutzait, J. E. Swagzdis, J. Jr. Flagiello, B. Y. Hwang, R. H. Dewey, H. Noguchi Pharmacokinetics of auranofin in animals. J. Rheumatol. 8 (1982) 90-98.
68. M. D. Smith, P. M. Brooks Gold compounds in rheumatic diseases. II. Med. J. Aust. 144 (1984) 77-81.
69. D. T. Walz, D. E. Griswold, M. J. Di Martino, E. E. Bumbier Pharmacokinetics of gold following administration of auranofin (SK+FD-39162) and myochrysine to rats. J. Rheumatol. 7 (1980) 820-824.
70. K. L. Blocka, H. E. Paulus, D. E. Furst Clinical pharmacokinetics of oral and injectable gold compounds. Clin. Pharmacokinet. 11 (1986) 133-143.

71. H. M. Rubinstein, A. A. Dietz Serum gold. II. Levels in rheumatoid arthritis. Ann. Rheum. Dis. 32 (1973) 128-132.

72. R. C. Gerber, H. E. Paulus, R. I. Jennrich, M. Lederer, R. Bluestone, W. H. Blahd, C.M. Pearson Gold kinetics following aurothiomalate therapy: use of a whole-body radiation counter. J. Lab. Clin. Med. 83 (1974) 778–789.

73. E. S. Waller, J. W. Massarella, J. E. Crout, G J. Yakatan, The half-life of gold sodium thiomalate. Arthritis Rheum. 22 (1979) 1418-1419.

74. D. E. Furst, S. H. Dromgoole Comparative pharmacokinetics of triethylphosphine gold (auranofin) and gold sodium thiomalate (GST). Clin. Rheumatol. 3 (1984) 17-24.

75. A. Hershko The Ubiquitin System for Protein Degradation and Some of Its Roles in the Control of the Cell-Division Cycle (Nobel Lecture). Angew. Chem. Int. Ed. 117 (2005) 6082-6094.

76. Y. Kulathu, D. Komander Atypical ubiquitylation - the unexplored world of polyubiquitin beyond Lys48 and Lys63 linkages. Nat. Rev. Mol. Cell. Biol. 13 (2012) 508-522.

77. M. J. Clague, S. Urbè Ubiquitin: same molecule, different degradation pathways. Cell 143 (2010) 682-685.

78. J. F. Trempe Reading the ubiquitin postal code. Curr. Opin. Struct. Biol. 21 (2011) 792-801.

79. A. Mani, E. P. Gelmann The ubiquitin-proteasome pathway and its role in cancer. J. Clin. Oncol. 23 (2005) 4776-4789.

80. R. Varadan, O. Walker, C. Pickart, D. Fushman Structural properties of polyubiquitin chains in solution. J. Mol. Biol. 324 (2002) 637-647.

81. G. Grasso, V. Lanza, G. Malgieri, R. Fattorusso, A. Pietropaolo, E. Rizzarelli, D. Milardi The insulin degrading enzyme activates ubiquitin and promotes the formation of K48 and K63 diubiquitin. Chem. Comm. 51 (2015) 15724-15727.
82. G. Arena, F. Bellia, G. Frasca, G. Grasso, V. Lanza, E. Rizzarelli, G. Tabbì, V. Zito, D. Milardi Inorganic stressors of ubiquitin. Inorg. Chem. 52 (2013) 9567-9573.
83. D. Twerenbold, D. Gerber, D. Gritti, Y. Gonin, A. Netuschill, F. Rossel, J. L. Vuilleumier Single molecule detector for mass spectrometry with mass independent detection efficiency. Proteomics 1 (2001) 66-69.
84. M. Karas, U. Bahr Laser desorption ionization mass spectrometry of large biomolecules. TrAC Trends Anal. Chem. 9 (1990) 321-325.
85. F. Hillenkamp, M. Karas, R. C. Beavis, B. T. Chait Matrix-assisted laser desorption/ionization mass spectrometry of biopolymers. Anal. Chem. 63 (1991) 1193A-1203A.
86. O. Yanes, J. Villanueva, E. Querol, F. X. Aviles Detection of non-covalent protein interactions by 'intensity fading' MALDI-TOF mass spectrometry: applications to proteases and protease inhibitors. Nat. Protoc. 2 (2007) 119-130.
87. O. Yanes, F. X. Aviles, P. Roepstorff, T. J. D. Jørgensen Exploring the “intensity fading” phenomenon in the study of noncovalent interactions by MALDI-TOF mass spectrometry. J. Am. Soc. Mass Spectrom. 18 (2007) 359-367.
88. B. A. Schulman, J. W. Harper Ubiquitin-like protein activation by E1 enzymes: the apex for downstream signalling pathways. Nat. Rev. Mol. Cell Biol. 10 (2009) 319-331.

89. S. Spreckelmeyer, C. Orvig, A. Casini Cellular Transport Mechanisms of Cytotoxic Metallodrugs: An Overview beyond Cisplatin. Molecules 19 (2014) 15584-15610.

90. M. Altaf, M. Monim-Ul-Mehboob, A.-N. Kawde, G. Corona, R. Larcher, M. Ogasawara, N. Casagrande, M. Celegato, C. Borghese, Z.H. Siddik, D. Aldinucci, A.A. Isab, New bipyridine gold(III) dithiocarbamate-containing complexes exerted a potent anticancer activity against cisplatin-resistant cancer cells independent of p53 status., Oncotarget. 8 (2017) 490–505.

91. M. Altaf, M. Monim-ul-Mehboob, A.A.A. Seliman, M. Sohail, M.I.M. Wazeer, A.A. Isab, L. Li, V. Dhuna, G. Bhatia, K. Dhuna, Synthesis, characterization and anticancer activity of gold(I) complexes that contain tri-tert-butylphosphine and dialkyl dithiocarbamate ligands, Eur. J. Med. Chem. 95 (2015) 464–472.

92. N. P. E. Barry, P.J. Sadler, 100 years of metal coordination chemistry: from Alfred Werner to anticancer metallodrugs. Pure Appl. Chem. 86 (2014) 1897-1910

93. K. Takahashi, P. Griem, C. Goebel, J. Gonzalez, E. Gleichmann The antirheumatic drug gold, a coin with two faces: Au(I) and Au(III). Desired and undesired effects on the immune system. Met. Based Drugs 1 (1994) 483-496.

94. G. F. Shaw III, S. Schraa, E. Gleichmann, Y. P.Grover, L. Dunemann, A. Jagarlamudi Redox chemistry and [Au(CN)2] in the formation of gold metabolites. Met. Based Drugs 1 (1994) 351-362.

95. D. Buac, S. Schmitt, G. Ventro, F. Rani Kona, Q. Ping Dou, Dithiocarbamate-based coordination compounds as potent proteasome inhibitors in human cancer cells, Mini-Reviews Med. Chem. 12 (2012) 1193–1201.

96. B. Cvek, Z. Dvorak, The value of proteasome inhibition in cancer. Can the old drug, disulfiram, have a bright new future as a novel proteasome inhibitor?, Drug Discov. Today. 13 (2008) 716–22.

Highlights

- Solubilization with β–CDs increases the stability and the bioavailability of AuL12
- AuL12 was able to block ubiquitin chain growth under cell-free conditions.
- AuL12 inhibits proteasome in cell with a potency similar to that of bortezomib
- AuL12 mechanism of action relies on an energy-dependent uptake.